

12

Distance Measurements: Continuous-Wave (CW)- and Pulsed Dipolar EPR

Sushil K. Misra and Jack H. Freed

12.1

Introduction

Information on long-range distances between selected sites is a prerequisite to understanding the detailed structure of complex systems. In NMR utilizing a spin label, it is possible to measure distances in the range between 8 Å to, at most, 25 Å. On the other hand, with EPR, distances in the range between about 10 and 90 Å can and have been measured. EPR spectroscopy may be the best practical technique for complex systems, since methods such as small-angle scattering, X-ray scattering and small-angle neutron scattering have insufficient contrast whereas fluorescence resonant energy transfer (FRET) lacks key virtues of EPR noted below. Distance measurements in EPR are based on exploitation of the dipolar interaction (DI), that depends on the distance between two paramagnetic probes, and which may be identical or may differ from each other, and are located at different spatial positions in the sample. They can be introduced using site-directed mutagenesis (also known as site-directed spin labeling; SDSL), a technique which enables the investigation of, for example, proteins and other biomolecules. In fact, the signature of the DI can be clearly seen in CW-EPR spectra under favorable circumstances for short distances. On the other hand, in pulsed EPR [hereafter referred to as pulsed dipolar spectroscopy; PDS], experiments can be designed specifically to clearly distinguish the dipolar interaction. The two commonly used PDS techniques are: (i) pulsed electron double resonance (PELDOR; this term was originally coined by the Russians, who first developed the technique), which is also referred to as double electron-electron resonance (DEER; this term was introduced later in the USA, and will be used hereafter in this chapter); and (ii) double quantum coherence (DQC)-EPR.

DEER requires an experimental arrangement which is relatively simple to implement and is currently available commercially. On the other hand, DQC requires instrumentation that can provide short, intense pulses and extensive “phase-cycling”. The quantitative results so obtained can be exploited to obtain distances, their distributions, and orientational correlations. Neither the DEER (PELDOR) nor DQC acronyms indicate that these techniques deal exclusively with dipolar

couplings; hence the acronym PDS will be used collectively hereafter for these techniques.

It is relevant at this point to compare distance measurements by PDS with those by the other commonly used techniques, specifically X-ray, NMR, and fluorescence resonance energy transfer (FRET). It should first be noted that PDS is often helped by—and provides information supplementary to—the structural information available from X-ray crystallography and NMR. One of the greatest virtues of using EPR is that one only requires trace amounts (in the case of proteins or biomolecules, from nanomoles to picomoles; Klug *et al.*, 2005; Bhatnagar *et al.*, 2010; Georgieva, *et al.*, 2010) of the sample due to its EPR spin sensitivity. EPR is also amenable to study in diverse environments, such as dilute solutions, micelles, lipid vesicles, native membranes, supported lipid bilayers. Such measurements are frequently not possible with NMR or X-ray crystallography, where one requires, for example, larger quantities of samples, high-quality crystals (for x-rays), as well as high solubility (for NMR), and smaller molecules (NMR). FRET is also used for distance measurements, as it is much more sensitive per fluorophore than EPR, and can operate at biological temperatures. That is, FRET can be applied to fluid solutions at room temperature, whereas the PDS-EPR experiments are conducted with frozen solutions. The main advantages of PDS over FRET are:

- The molecular size of the probes is smaller, so that the original structure is less distorted. In PDS, there is often used a methanethiosulfonate spin label (MTSSL), which introduces only a small perturbation to the structure and function of the protein. Since the nitroxides, used in PDS, are smaller in size than most fluorescent labels used in FRET, there is less uncertainty in their positions relative to the backbone of the protein.
- Attaching two similar paramagnetic labels synthetically is less demanding than attaching two different donor and acceptor labels.
- The EPR technique can also be applied to opaque materials.
- The distances between the nitroxide spin-labels used in EPR is determined more accurately, as they are directly obtained from frequency measurements. This contrast to the distances between chromophores used in FRET, where there exist uncertainties in the parameter κ^2 used for distance determination.
- Also, the distance distributions are readily obtained in PDS-EPR.

This chapter is organized as follows. The theory for distance measurements in EPR using the dipolar interaction is provided in Section 12.2, the CW-EPR methods used for distance determination are discussed in Section 12.3, and pulsed dipolar techniques in general are detailed in Section 12.4. The details of three- four-pulse DEER techniques, and their merits and disadvantages as compared to CW-EPR and FRET, are described in Section 12.5. The density matrix calculations of echo signals for three- and four-pulse DEER sequences are given in detail in Appendices 12.I and 12.II, respectively. The DQC technique is described in Section 12.6, along with the density-matrix evolution algorithm used to calculate the DQC signal, while

sensitivity considerations and their multifrequency aspects are discussed in Section 12.7. The subject of distance distributions, including Tikhonov regularization, is covered in Section 12.8, and the pertinent literature is reviewed in Section 12.9.

12.2

The Dipolar Interaction and Distance Measurements

The general expression for a dipolar interaction between two magnetic moments is given later in this chapter (see also Chapter 10.) For EPR, the relevant part of the dipolar interaction between two electrons, 1 and 2, treated as point dipoles, can be expressed in frequency units as follows (Borbát and Freed, 2007):

$$\frac{H_{dd}}{\hbar} = \frac{\gamma_e^2 \hbar}{r^3} (3 \cos^2 \theta - 1) \left[S_{1z} S_{2z} - \frac{1}{4} (S_1^+ S_2^- + S_1^- S_2^+) \right]. \quad (12.1)$$

In Equation 12.1, γ_e is the electronic gyromagnetic ratio; r is the distance between the two electrons; θ is the angle between the vector joining the two electrons and the external magnetic field; and S_1, S_2 are the two electron spins, whose subscripts may be x, y , or z , indicating the components along the three axes, and the superscripts $+$ and $-$ indicating the raising and lowering operators, respectively: $S_i^\pm = S_{ix} \pm i S_{iy}$; $i = 1, 2$. The first term inside the square brackets is called the *secular* term, whereas the second term is called the *pseudosecular* term. The *non-secular* term is omitted for high fields and frozen samples. It is clear from Equation 12.1 that, from a knowledge of the expectation value of H_{dd} , one can estimate the distance, r , between the spin probes.

As a consequence of Equation 12.1, the CW-EPR line for each spin is split into two due to the dipolar interaction. The splitting of this doublet, $|A(r, \theta)|$, which can be expressed from Equation 12.1 as:

$$A(r, \theta) = \omega_d (1 - 3 \cos^2 \theta), \quad (12.2)$$

In Equation 12.2 the value of ω_d depends on whether the spins are “unlike” or “like”. $A(r, \theta)$ also depends on the angle θ , varying over the range of values from $-2\omega_d$ ($\theta = 0^\circ$) to ω_d ($\theta = 90^\circ$).

12.2.1

Unlike Spins

This is the case when $\omega_d \ll |\omega_1 - \omega_2|$, where ω_1 and ω_2 are the resonant frequencies of the two electron spins in the absence of dipolar coupling. Equation 12.2 is obtained when only the secular term in Equation 12.1 is taken into account, and ignoring the second term in square brackets (pseudosecular term). For this case:

$$\omega_d = \gamma_e^2 \hbar / r^3, \quad (12.3)$$

It should be noted that, in the case of nitroxide spin labels, there usually exists the situation of “unlike” spins due to the different orientations of the magnetic,

g , and A (hyperfine) tensors with respect to the external magnetic field, of any two nitroxides. The “unlike” limit is valid for $r \geq 20 \text{ \AA}$.

12.2.2

Like Spins

Here, $\omega_i \gg |\omega_1 - \omega_2|$, and both the secular and pseudosecular terms in Equation 12.1 are taken into account, so that

$$\omega_d = 3\gamma_e^2 \hbar / 2r^3, \quad (12.4)$$

12.2.3

Intermediate Case

Here, $\omega_i \approx |\omega_1 - \omega_2|$, and one has to carry out a careful simulation of the spectrum taking into account both the secular and pseudosecular terms in Equation 12.1, as well as using the full spin Hamiltonian.

Distance measurements in EPR are made by either using a CW method or pulsed techniques. These are described as follows.

12.3

CW EPR Method to Measure Distances

In the past, nitroxide spin probes have been the most popular CW-EPR probes for distance determination with regards to their dipolar interaction, mainly because they are stable and easy to attach to systems (such as cysteine residues in proteins). Their powder spectra are governed by the inhomogeneous broadenings, which differ from site to site, due to the variation of nitrogen hyperfine (hf)- and g -tensors largely from the $\cos\theta$ angular variation in eq. 12.1, as well as to unresolved proton superhyperfine couplings. Current CW methods include techniques based on calculating the ratios of peak intensities (Kokorin *et al.*, 1972; Sun *et al.*, 1999), the relative intensity of half-field transition (Eaton *et al.*, 1983), Fourier deconvolution of dipolar interactions (Rabenstein and Shin, 1995), and the computer simulation of lineshapes (Hustedt *et al.*, 1993). All of these methods depend on the observation of reasonably significant broadening of the lineshape due to electron–electron dipolar interaction, limited by inhomogeneous line broadening due to unresolved hyperfine couplings, g -anisotropy, and relaxation. For distances of up to 20 \AA between spin labels, the dipolar broadening is still measurable for CW-EPR. Since, the dipolar interaction between nitroxide spin labels produces a relatively small broadening effect, as compared to that due to other interactions, it must be extracted from the CW-EPR powder spectra, either by a rigorous multi-parameter fit (Hustedt *et al.*, 1997), or by a spectral deconvolution (Rabenstein and Shin, 1995). For these procedures, one also needs spectra from a singly-labeled sample as a reference for the background broadening, although this will produce

complications that are compounded by incomplete spin-labeling (as discussed by Persson *et al.*, 2001). As the magnitude of the dipolar coupling increases—specifically for distances less than 15 Å, when it becomes comparable to other inhomogeneous spectral broadenings—it can be more easily deduced from CW-EPR spectra. As a consequence, CW-EPR is practical for shorter distances up to a maximum of about 15–20 Å, with the more reliable values being obtained for distances less than 15 Å (Persson *et al.*, 2001); in particular, this applies to half-field transitions (5–10 Å), lineshape simulations (up to 15 Å), and Fourier deconvolution (8–20 Å). On the other hand, with PDS (see below) one can measure distances in the range of 10 to 90 Å currently.

12.4 Pulsed Dipolar EPR Spectroscopy (PDS)

For smaller dipolar interactions corresponding to longer distances, pulsed techniques are utilized where the distance scale is limited by the rate constant (i.e., inverse of phase memory time, T_M) for echo dephasing, which is much smaller than the inhomogeneously broadened continuous-wave linewidth. This allows for dipolar oscillations in the time domain corresponding to much lower frequencies, hence longer distances (cf. eq. 12.3) than can be measured by cw means. Currently, two PDS techniques are in use, namely DEER (that is, PELDOR) and DQC. Three-pulse DEER was developed originally as an improvement over spin-echoes to utilize the dipolar interaction to measure distances between spin probes, whereas the more recent, more improved techniques are four-pulse DEER and DQC. The spectroscopic details of these techniques are detailed in Chapter 4, Section 4.4, whereas the theoretical details of their principles of operation with regards to distance determination are described below. It should be noted here that in DEER one purposely excites only a part of the spectrum using pulses that are weaker and of relatively longer duration. This means that different parts of the CW-EPR spectrum, resonating at different frequencies ω_A and ω_B , can be excited separately. In contrast, in the case of DQC, the pulses are intense and of short duration, so that the entire CW-EPR spectrum is excited under the action of the various pulses at the same frequency applied at different times. In PDS, a spin-echo is detected, in which the inhomogeneous spectral broadenings are canceled out due to refocusing. The temporal evolution of this spin-echo is governed by T_M , the phase relaxation time, which is a weaker effect than typical inhomogeneous broadenings. It is important to note here that the dipolar and exchange couplings are discriminated from all other interactions by employing the suitable pulsed sequences. In this manner, the signal caused by the presence of single-labeled molecules is obviated. Although, the direct signal from single-labeled molecules is filtered out in PDS, they can still contribute to the background *intermolecular* dipolar signal; however, the latter can be minimized by working at low concentrations.

Pulsed dipolar spectroscopy is now used routinely to measure distances greater than 15–20 (Banham *et al.*, 2006; Borbat *et al.*, 2006; Borbat *et al.*, 2004; Cai *et al.*,

2006; Jeschke, 2002; Park *et al.*, 2006), to distances as long as 60 to 90 Å (Georgieva *et al.*, 2008; Georgieva, *et al.*, 2010; Bhatanagar, *et al.* 2010), and is also quite efficient down to 10 Å (Fafarman *et al.*, 2007; Borbat and Freed, 2007), significantly overlapping the range covered by CW-EPR. However, unlike CW-EPR, PDS is much less susceptible to inefficient labeling, and it can also readily yield distance distributions; its sensitivity is also very high, as the following discussion reveals.

The main goal of PDS is to solve structures of biomolecules by providing distance constraints. It has been exploited to accomplish the following: (i) single-distance measurements; (ii) multiple-distance measurements; (iii) triangulation; (iv) oligomeric proteins; (v) protein complexes; (vi) embedding PDS constraints and rigid-body modeling; (vii) investigation of difficult labeling cases; and (viii) structural and conformational heterogeneity, protein folding (Borbat and Freed, 2007).

12.5

Double Electron–Electron Resonance (DEER)

DEER (also known as PELDOR), was developed in Russia during the 1980s by Milov and collaborators (Milov, Salikhov, and Shirov, 1981; Milov, Ponomarev, and Tsvetkov, 1984) with improvements introduced in 1993 (Larsen and Singel, 1993). Years later (Martin *et al.*, 1998; Narr, Godt, and Jeschke, 2002), a deadtime-free variant of the method was proposed—termed four-pulse DEER (Pannier *et al.*, 2000)—which enables commercial instrumentation, and with advances in site-directed spin labeling, resulted in a widespread application to structural biology.

In order to describe the DEER experiment, an isolated coupled pair of spins in a (disordered) solid must first be considered. The DEER signal is a modulation of the echo amplitude of the observing spins, S_1 , resonating at the frequency, ω_1 , by another set of spins, S_2 , called “pumping” spins, resonating at the frequency, ω_2 . When excited by respective microwave pulses, the spins S_1 experience the dipolar field generated by the spins S_2 ; the echo of spins S_1 will then be modulated in a manner that is a function of the time at which spins S_2 are excited. The resulting DEER signal can be expressed as a product of two parts: (i) decay due to the intermolecular interactions of the unpaired spins; and (ii) the periodic oscillations generated by the intramolecular dipolar interactions of the paired spins, expressed as

$$I(t) = I_{\text{intra}}(t) \times I_{\text{inter}}(t) \quad (12.5)$$

The modulation of the echo arises from the observing spins S_1 experiencing a local magnetic field arising from the dipolar interactions with the nearby spins S_2 . Since the direction of this field at S_1 is determined by the spin state of the coupled spin, S_2 , changing the latter selectively affects the contribution of the dipolar field to the total magnetic field at S_1 .

Distance measurements between two spins involve excitations of both S_1 and S_2 spins. The expected spectrum of the spin pair consists of a pair of doublets, centered at ω_1 and ω_2 , each with equal splitting due to the dipolar interaction, as shown in Figure 12.1.

We write eqs. 12.2 and 12.3 for dipolar splitting, ω_{12} , between two “unlike” spins S_1 and S_2 at distance r is given by:

$$A(r, \theta) \equiv \omega_{12} = \frac{\mu_B^2 g_1 g_2}{\hbar r^3} (3 \cos^2 \theta - 1), \quad (12.6)$$

where μ_B is the Bohr magneton, g_1 and g_2 are the g -factors for spins 1 and 2, as shown in Figure 12.1a. For the samples randomly distributed with respect to the field, the integration of ω_{12} over the angle θ on the unit sphere produces a symmetric Pake pattern, in which the singularities ($\theta = 0^\circ$) are separated by $2 \frac{\mu_B^2 g_1 g_2}{\hbar r^3}$, as shown in Figure 12.1b.

Distance measurements between two spins involve excitations of both S_1 and S_2 spins. The expected spectrum of the spin pair consists of a pair of doublets, centered at ω_1 and ω_2 , each with equal splitting, ω_{ee} , due to the dipolar interaction, as shown in Figure 12.2.

The pulse exciting the S_1 spins is called the “observer” pulse, and that exciting the S_2 spins is called the “pump” pulse. The pulses ω_1 and ω_2 must be sufficiently

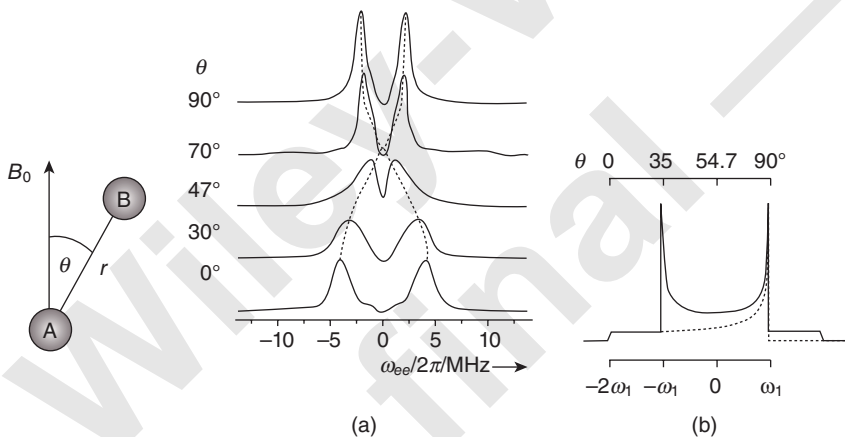


Figure 12.1 (a) The dependence of the dipolar spectrum on the angle θ between the magnetic field direction and the spin–spin vector; (b) Simulated Pake pattern for an isotropic sample. The θ scale refers to one line of the dipolar doublet. Adapted from Bhatnagar (2005).



Figure 12.2 EPR line spectrum of a pair of coupled electron spins consisting of two doublets. Adapted from Bhatnagar (2005).

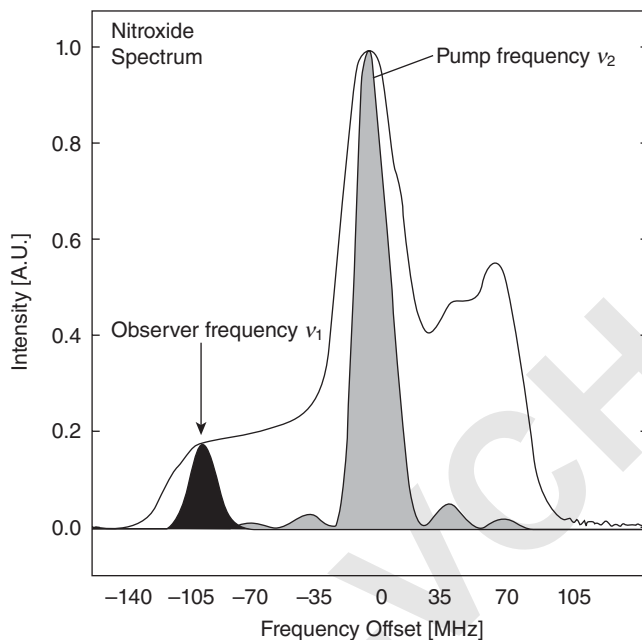


Figure 12.3 Excitation profiles due to pump and observer pulses in a nitroxide spectrum. Adapted from Pannier *et al.* (2000).

small that the excite the two levels of the doublet of the respective spin, S_1 or S_2 . In a DEER sequence, one monitors the observer pulse when a pump pulse is applied at a variable time in between the $\pi/2$ and π observer pulses. For the selective excitation of S_1 and S_2 spins, it is necessary that $|\omega_1 - \omega_2|$ be sufficiently large and the pulses weak enough to avoid overlap. In most cases, two pulses at different frequencies can be applied to avoid overlap if the total width of the EPR spectrum is more than 50 MHz (Jeschke, 2002). In the case of nitroxides, a difference of 60 MHz in the observer and pump frequencies is sufficient to avoid overlap of excitation ranges (Jeschke, Pannier, and Spiess, 2000); an example of this is shown in Figure 12.3.

12.5.1

Orientation-Selection Considerations in DEER

The Pake pattern in the frequency domain for an isotropic sample is shown in Figure 12.3b. In practice, when the pulses are not sufficiently intense and narrow to excite the whole spectrum, this is not obtained, and only parts of the nitroxide spectrum will be excited, leading to “orientation selection” of the probe. The most commonly used probe, the nitroxide radical, exists in many different orientations in a disordered sample. When a pulse is applied, not all the orientations are equally

excited, so that, only a part of the spectrum corresponding to the S_1 and S_2 spins is excited. These selected orientations for S_1 and S_2 spins may be correlated with each other by a certain set of angles between the vector connecting the electron pairs and the static field direction. Thus, the angle θ in Equation 12.1 does not necessarily represent an isotropic distribution (Jeschke, Pannier, and Spiess, 2000). The effect of orientation selection on the signal is significant if the excitation bandwidth is much smaller than the anisotropy of the g or hyperfine tensor. In such cases, the orientation selection may suppress the $\theta = 0$ feature from the Pake pattern, as the observer and pump frequencies are clearly distinct from each other.

12.5.2

Three-Pulse DEER

The three-pulse DEER sequence, which was originally developed by Milov, Salikhov, and Shirov (1981), consists of a two-pulse Hahn echo sequence $\pi/2 - \tau' - \pi$ at the “observer” frequency, as shown in the upper part of Figure 12.4. The observer frequency is kept fixed, while an additional π pulse at the “pump” frequency is applied after a delay, τ , which is variable, subsequent to the observer frequency pulse at the time $t = 0$ (as shown in the lower part of Figure 12.4). The signal is obtained by recording the Hahn echo amplitude at the observer frequency as a function of τ .

The three-pulse DEER sequence is:

$$X_1(\pi/2) - \tau - X_2(\pi/2) - (\tau' - \tau) - X_1(\pi) - (t - \tau')$$

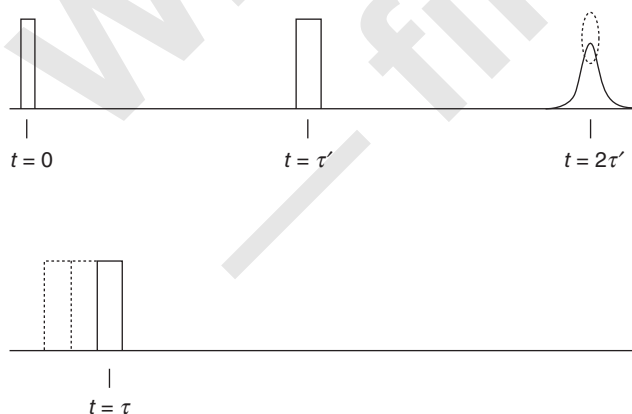


Figure 12.4 A schematic drawing of the three-pulse DEER sequence, consisting of a refocused echo sequence at the observer frequency ν_1 and of a π pulse at the pump frequency ν_2 . (Adapted from Larsen and Singel (1993).)

In Appendix 12.I are given the details of the calculation of a three-pulse DEER signal using a density-matrix approach. The following three-pulse echo amplitude, given by the expectation value of S_1^+ , is calculated in Appendix 12.I:

$$\langle S_1^+(2\tau') \rangle = -iI_0 \cos(\omega_{12}\tau). \quad (12.7)$$

Equation 12.7 contains the dipolar interaction between two spins, ω_{12} . The cosine Fourier transformation of this modulation will give rise to a Pake pattern when the exchange coupling is ignored. The details of the Pake pattern can be exploited to estimate the distance between two spins by extracting the values of $\nu_{ee} = \omega_{ee}/2\pi$ for $\theta = 90^\circ$ from the Pake pattern. Here $\omega_{ee} = \omega_d (3 \cos^2\theta - 1) + J$, where J is the exchange interaction between the two spins (which will be neglected here), and ω_d is defined by Equation 12.2. The distance is given by the formula (Larsen and Singel, 1993):

$$r = (53.041 \text{ MHz}/\nu_{ee})^{1/3} \text{ nm}$$

The derivation of the echo amplitude given by Equation 12.6 is based on the assumption of an isolated pair of spins. In reality, a sample is characterized by a statistical distribution of spins. As a consequence, its observed spectrum is the superposition of the various spectra associated with all the constituents of the sample. The DEER spectrum is affected by both the remote (intermolecular) and near (intra-molecular)-pair dipolar interactions. The contribution due to the near pairs typically exhibits oscillatory behavior with time. On the other hand, the interactions due to remote pairs are governed by broadly distributed dipolar couplings that have the effect of a damping of the time-dependent signal. The damping and oscillatory components of the signal are clearly seen in Figure 12.5, which

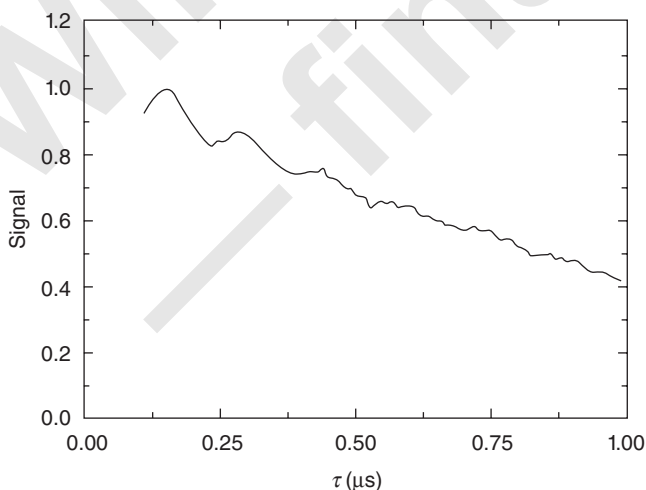


Figure 12.5 Time domain data (spin-echo envelope) of a 2 mM, frozen toluene solution of a biradical at 77 K from a three-pulse DEER sequence. Adapted from Larsen and Singel (1993).

shows an observed three-pulse DEER spectrum. Finally, a three-pulse DEER signal is expressed by the following expression (Klauder and Anderson, 1962; Borbat and Freed, 2007):

$$V(t) = V_0 e^{-kCF_B t} [1 - \lambda \{1 - u(\omega_d t)\}];$$

$$u(\omega_d t) = \int_0^{\pi/2} \cos[\omega_d (1 - 3\cos^2 \theta)t] d(\cos \theta) \quad (12.8)$$

where, C is the concentration of sample; F_B is the fraction of spins S_2 excited by the pump pulse; λ is the modulation-depth parameter that depends on the fraction of S_1 spins excited by the observer pulse, and $k = 8\pi^2 \mu_B^2 g_1 g_2 / (9\sqrt{3}\hbar)$.

According to Equation 12.8 for $V(t)$, it is seen that in order to avoid overdamping of the DEER signal, one should use a small bulk concentration, C .

12.5.3

Four-Pulse DEER

This was developed by Pannier *et al.* (2000). In the three-pulse case there are dead-time effects, as well as pulse overlap issues. Thus, it is not possible to measure signals from spin pairs, which have such a distance distribution that they decay completely during the microwave pulses of the order of few tens of nanoseconds. Also, in practice, the signal is distorted for times less than the dead time, which is typically in the range from 30 to 100 ns. It is possible to eliminate these dead time issues and achieve “dead-time free” signals by using an additional pulse. This is accomplished in the four-pulse DEER sequence, as shown in Figure 12.6. This four-pulse sequence can be expressed schematically by the following scheme: $X_1(\pi/2) \dots \tau_1 \dots X_1(\pi) \dots t \dots X_2(\pi/2) \dots (\tau_1 + \tau_2 - t) \dots X_1(\pi) \dots (t' - \tau_2)$. The echo signal detected is the expectation value $\langle I^+(t) \rangle$. The effect of the pulses is described as follows. When the observing spins S_1 , are oriented by the $\pi/2$ pulse along the γ -axis following the first microwave pulse of frequency ω_1 , which tips

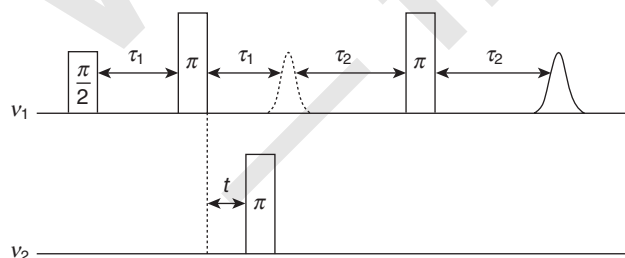


Figure 12.6 Four-pulse DEER sequence, which produces a refocused echo sequence for the observer spins. A π pulse at the pump frequency ν_2 is applied at time t after the application of the first π pulse to observer spins. The second π pulse at the

observer frequency is applied after the time τ_2 subsequent to the formation of the first echo of observer spins. The time t is varied, whereas τ_1 and τ_2 are fixed. Adapted from Bhatnagar (2005) and Pannier *et al.* (2000).

these spins into the xy -plane, they precess with the angular rate of ω_1 . Spins S_1 at different sites experience slightly different angular rates due to the presence of field inhomogeneities and different resonance fields, which dephase the spins S_1 from each other. For example, the dipolar field due to nearby spins S_2 adds or subtracts its angular rate by $\pm\frac{1}{2}\omega_{12}$, depending on the spin state of spins S_2 . A spin echo is created when a π -pulse is applied to spins S_1 , which reverses the dephasing and refocuses spin S_1 along the x -axis. This echo obtained by application of $\pi/2$ - π pulse sequence, which is called a “Hahn echo”, plays a key role in most pulsed EPR experiments. After the echo, spins S_1 continue to precess in the xy -plane, and the subsequent π pulse again refocuses, leading to the “refocussed echo,” but with a smaller amplitude as the phase coherence continues to be lost due to the spin relaxation. The dipolar contribution is now reversed in its superimposition on the total field experienced by spins S_1 , by applying a π pulse to spins S_2 , which is known as a “pumping” or “ELDOR” pulse (as it is the second frequency to excite spins S_2). It reverses the direction of S_2 spins, which, in turn, reverses the dipolar contribution experienced by the S_1 spins from $+\frac{1}{2}\omega_{12}$ to $-\frac{1}{2}\omega_{12}$ and *vice versa*. S_1 spins accrue a phase lag due to the change of the dipolar contribution to the angular rate of precession of spins A in between the two π -pulses; these are then no longer refocused along the x -axis and this results in a decrease in the intensity of the echo. The accrued phase lag reflects the strength of the dipolar interactions, ω_{12} (as given above in Equation 12.6), as well as the time at which the pumping pulse is applied, which determines how long spins S_1 experience the dipolar field $+\frac{1}{2}\omega_{12}$ versus $-\frac{1}{2}\omega_{12}$. The total accrued phase difference is $\omega_{12}(\tau - t)$, where τ is the interval between the $\pi/2$ and π pulses and t is the timing of the pumping pulse with respect to the initial echo, which is 2τ after the first $\pi/2$ pulse. The DEER signal is the modulation of the echo intensity as a function of the time of application of the pumping pulse between the π pulses. Finally, the echo intensity oscillates as

$$I_{\text{intra}}(t) = I_0 \cos(\omega_{12}\{\tau_1 - t\}), \quad (12.9)$$

where I_0 is the echo in the absence of the dipolar interactions.

The density-matrix treatment of a four-pulse DEER sequence is given in Appendix 12.II, where the following result is calculated for the echo signal for an isolated pair of spins:

$$\langle I^+(2\tau_1 + 2\tau_2) \rangle = iI_0 \cos(a[t - \tau_1]) = iI_0 \cos(\omega_d[t - \tau_1]) \quad (12.10)$$

The four-pulse DEER signal consists of a damping component when averaged over a real sample, taking into account statistical distributions of the various pairs of spins, similar to that considered for the three-pulse DEER sequence. To be used in Equation 12.5, for a homogeneous distribution of spins, such as in a glass solution (Milov, Salikhov, and Shirov, 1981; Milov, Ponomarev, and Tsvetkov, 1984), one has:

$$I_{\text{inter}}(t) = \exp(-kCF_B|\tau_1 - t|), \quad (12.11)$$

where C is the concentration of spins S_1 that interact with each other via intermolecular interactions, F_B is the fraction of spins B excited by the pumping microwave with frequency, ν_p , and k is given by:

$$k = \frac{8\pi^2 \mu_B^2 g_A g_B}{9\sqrt{3}\hbar}.$$

It is also superimposed by an oscillatory part, as shown in Figure 12.7, similar to that found in a three-pulse sequence. However, the refocused echo amplitude is smaller in the four-pulse sequence as compared to that due to a three-pulse sequence, since here an additional pulse has been introduced, so a longer time evolution is required for the refocused echo. On the other hand, since the values of $(t - \tau_1)$ are smaller here as compared to that due to a three-pulse sequence, they lead to enhanced modulation depths.

The four-pulse DEER signals, as obtained from six oligonucleotides, are shown in Figures 12.8a and b (Schiemann *et al.*, 2004). These reveal that time dependencies of five doubly labeled oligonucleotides DNA1–DNA5 show oscillations except for DNA 6, which is singly labeled, missing the second spin for dipolar interaction. The echo decay observed for all DNA results from intramolecular spin–spin coupling. The Fourier transform of the DEER signal due to DNA1 in the frequency domain, as obtained after subtraction of echo decay, is shown in Figure 12.9; here, the Pake pattern is clearly visible, allowing the distances to be calculated in the same way as in a three-pulse DEER experiment.

12.5.4

Merits and Limitations of DEER as Compared to CW-EPR and FRET

These are as follows:

- The DEER method has the advantage that the characteristic oscillations in the signal due to the dipolar interaction are obtained only from doubly labeled protein; there is no contribution from singly labeled protein. Further, the rate

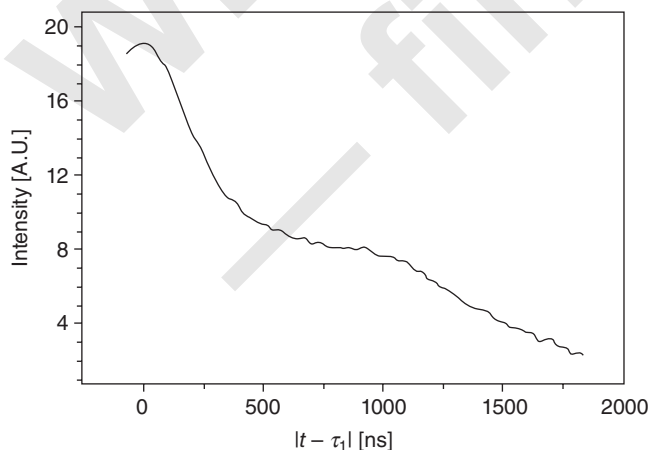


Figure 12.7 Experimental time domain signal obtained from four-pulse DEER experiment. Adapted from Bhatnagar (2005).

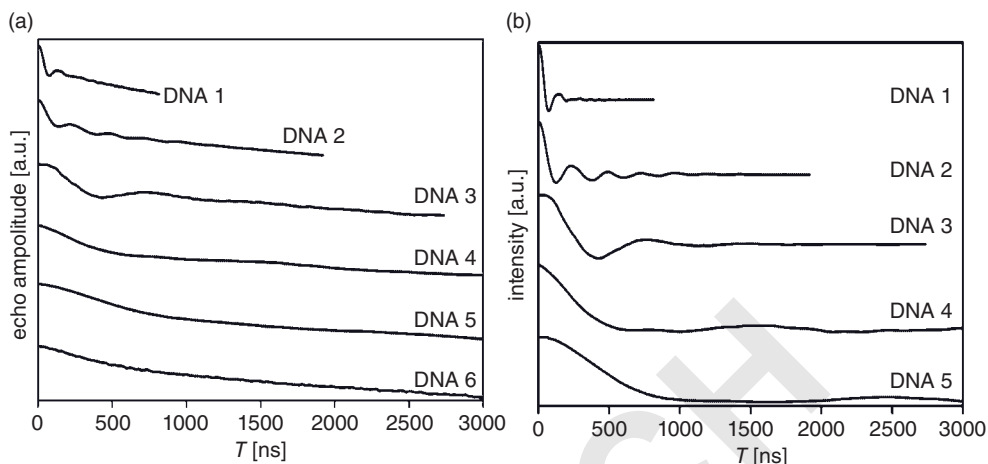


Figure 12.8 (a) DEER time traces of DNAs 1–6; (b) DEER time traces of DNAs 1–5 after subtraction of the echo decay. Adapted from Schiemann *et al.* (2004).

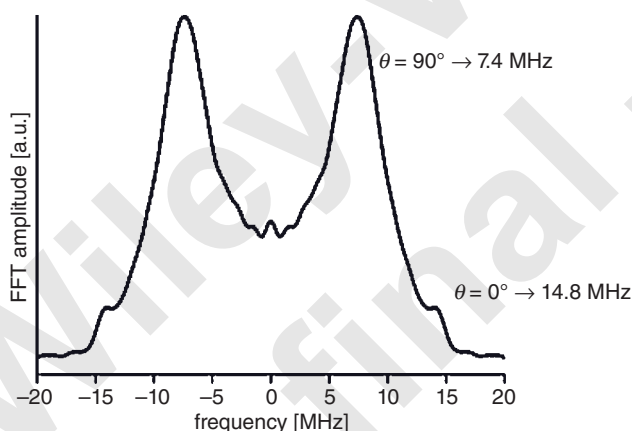


Figure 12.9 Fourier-transformed spectrum for DNA 1. Adapted from Schiemann *et al.* (2004).

at which the oscillation is damped provides a direct indication of the widths of distance distribution, which can only be obtained from CW lineshapes by either simulation or deconvolution.

- Distance measurements by DEER are limited on the upper side by the T_2 relaxation time, whereas the lower limit of ca. 15–20 Å is determined by the failure of the weaker DEER pulses to irradiate both parts of the Pake doublet, whereas DQC does not have this limitation, see Figure 12.10.
- One can measure larger distances, up to 80 Å (see Figure 12.11, from Georgieva *et al.*, 2010), with DEER, than are possible with CW-EPR.

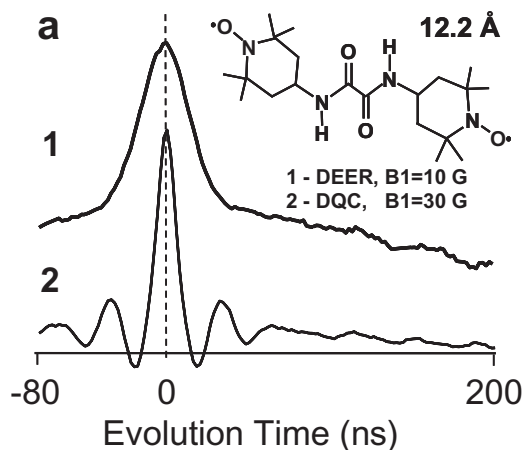


Figure 12.10 The challenges of short distances. DQC and DEER were applied to a rigid 12.2 Å nitroxide biradical. Detection pulses in DEER were 16/32/32ns, the pumping pulse was 18ns (B₁~10G). This is found to be insufficient to properly excite the dipolar spectrum. DQC using 6.2ns π -pulse

(B₁~30G) develops the ~30MHz oscillations very cleanly. The longer pulses of DEER lead to a spread in the refocusing point of different spin packets, and the weaker B₁, both smear out the high-frequency dipolar oscillations. (From Borbat and Freed, 2007).

- A four-pulse DEER sequence is especially suitable when there exist broad distributions of small and intermediate distances. Furthermore, no comparison with the spectra due to monoradicals is required in DEER, unlike that in CW-EPR.
- As mentioned above, in DEER, the difference $|\omega_1 - \omega_2|$ needs to be significant in order to accomplish the required selective excitation. This restricts the use of those probes which satisfy the condition for DEER.
- Unlike FRET, orientation-dependence in DEER is well defined. In contrast, with FRET one can measure distances at the single-molecule scale, whereas at least 10 pmol of sample is required for DEER distance measurements.

12.6 Six-Pulse DQC

This technique for distance measurements was developed at Cornell University by Freed and coworkers (Freed, 2000; Borbat *et al.*, 2001; Borbat, Mchaourab, and Freed, 2002; Borbat and Freed, 1999; Borbat and Freed, 2000). It is superior in a number of ways to DEER, but requires more intense microwave pulses. These include greater sensitivity especially for low concentration samples since (nearly) all the spins are excited; absence of orientational effects in its standard 1D version; filtering of single quantum signals and other noise by the double quantum filter; and the ability to obtain good results for distances as short as 10 Å. (See

Figure 12.11, from Borbat and Freed, 2007.) The double quantum coherence phenomenon has been extensively used in NMR (Ernst, Bodenhausen and Wokaun, 1987). We show in Figure 12.12 the six pulse sequence used in DQC-ESR. It transforms the initial density matrix under the successive action of six pulses, and six subsequent free-evolutions. In the ideal limit of perfect hard pulses, one may readily derive a simple expression for DQC-ESR by the product operator method analogous to those given in Appendix II.1 and II.2 for DEER (Borbat and Freed, 1999; 2000). It yields a cosine expression for the signal similar to those of Equations 12.7 and 12.10 for DEER (cf. Figure 12.12 caption). The following discussion is mostly taken from the recent publication on rigorous six-pulse DQC simulations by Misra, Borbat, and Freed (2009).

When a sample containing bilabeled proteins is subjected to a sufficiently strong microwave pulse, the nitroxide EPR spectrum is (almost) uniformly excited, and any orientational selection is (largely) suppressed; that is, it does not modify the

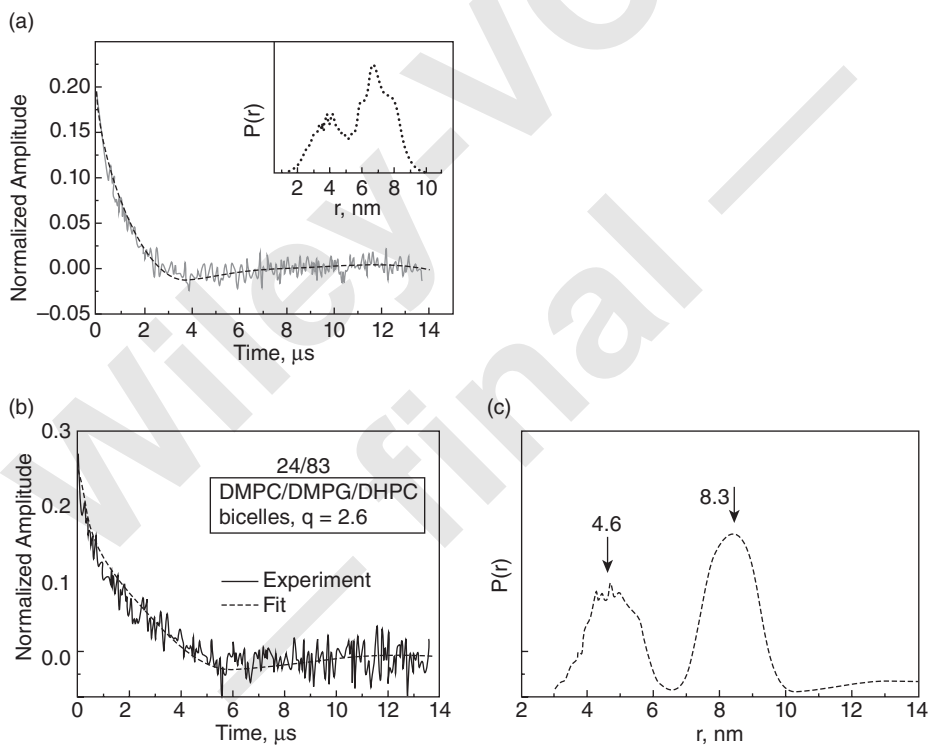


Figure 12.11 (a) The experimental time-domain data and distance distribution for 70% deuterated A30P alpha-synuclein (αS) mutant spin-labeled at positions 24 and 72 and reconstituted in micellar SDS-d25 using deuterated NMR buffer. (b) The experimental time-domain data (green) for 70% deuterated WT αS spin-labeled at positions 24 and 83 and

reconstituted into bicelles. The fit (red) is based on distance distribution (c) produced by Maximum Entropy Method (MEM). Protein deuteration allowed recording dipolar signal on the time scale as long as 14 μs . (Distribution centered at 4.6 nm in C due to protein in solution unassociated with bicelles.) (From Georgieva *et al.*, 2010).

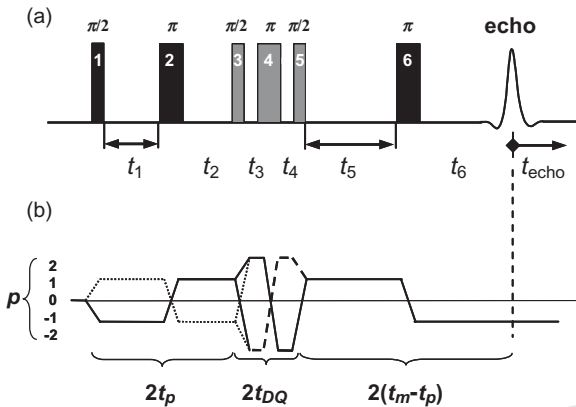


Figure 12.12 (a) The six-pulse DQC sequence; (b) Here, the coherence pathways correspond with the pulses shown in (a), in that a transition from one ρ state to another ρ state is generated by a pulse; the horizontal lines show coherence orders during the evolutions in the absence of a pulse. As for the timing between the various pulses the following is noted. The time interval $t_1 = t_2 = t_p$ is increased in equal steps, Δt_p , typically ranging from 1 to 10 ns, over a period of $t_m = t_p t_5$ (200–4000 ns in this case). The time $t_3 = t_4 = t_{DQ}$ is kept fixed, typically at 20 ns; $t_5 = t_6$ is stepped by $-\Delta t_p$ to maintain a constant t_m ; this starts from the initial time t_m . The echo signal is recorded in a window $t_w \sim 80$ –160 ns, centered at a time delay $2t_m + 2t_{DQ}$ after the first pulse—that is, at

about $t_6 = t_m$ after the sixth pulse. Note that the width of the echo sampling window limits the minimal values of t_6 and t_p by about $t_w/2$ and their maximum values to $(t_m - t_w/2)$. The dipolar evolution is recorded as a symmetric signal with respect to $t_{dip} \equiv t_m - 2t_p$ over the range of $\pm t_m$ in steps of $2\Delta t_p$. $t_{dip} = 0$ when the pulse separations are $t_1 = t_2 = t_5$. In practice, t_p starts with t_{p0} (~ 400 ns in this case), so that the last pulse and the echo window do not overlap. A simple analysis shows that the 1D signal goes as: $\cos \omega_d t_m - \cos \omega_d t_{dip}$. The signal in the 2-D DQC experiment is recorded (or computed) over $\pm (t_m - t_{p0})$, with t_{p0} always greater than $t_w/2$. Adapted from Misra, Borbat, and Freed (2009).

echo amplitude (except for the effect of pseudosecular dipolar terms, which is essential for short distances). Also, in high B_1 -fields, the effect of dipolar coupling during the pulses becomes relatively weak. Therefore, for not very short distances and in sufficiently strong rf excitation fields (B_1 s), the information on orientations of the magnetic tensors of the spin-label moieties, is virtually excluded from the time-domain dipolar evolution of the echo amplitude. However, as shown by Borbat and Freed (2000) and Misra, Borbat, and Freed (2009), it is still retained in the spin-echo evolution, and can be retrieved by recording the 2-D time-domain data as a function of the spin-echo time (t_{echo}) and the dipolar evolution time (t_{dip}). This can then be converted into a two-dimensional Fourier transform (2-D-FT) spectrum which, after making a “shear” transformation (Lee, Budil, and Freed, 1994), separates the dipolar dimension from the spectral dimension. Rigorous computations of 1-D and 2-D signals were carried out by Misra, Borbat, and Freed (2009), some of which are presented here. Efficient but approximate analytical expressions to this end were developed for 1-D signals by Borbat and Freed (2000) (see Appendix 12.V), by omitting the dipolar coupling during the pulses and assuming an ideal double-quantum (DQ) filter (cf. Figure 12.10, pulses 3, 4, and

5). Whereas, such expressions are quite useful for practical purposes and are computationally very efficient, they do not always supplant the rigorous calculations, especially in the case of short distances, for example, less than 15.0 Å. Numerical simulations of 1-D spectra were first carried out rigorously using these new codes in order to test the nature and extent of deviations from the exact results, and to establish the scope of applicability. The pulse propagators are calculated, using accurate numerical diagonalizations of the Hamiltonians involved. Although the computational approach is necessarily time-consuming, it does provide useful insights into the features of DQC spectroscopy.

12.6.1

Theoretical Background and Computation of Six-Pulse DQC Signal

The six-pulse DQC sequence is shown in Figure 12.10, indicating the pulse pattern and the relevant coherence pathways (Borbat and Freed, 1999; Borbat and Freed, 2000). The computational method for 1-D and 2-D-DQC spectra is outlined as follows.

The initial density matrix operator in thermal equilibrium for the two nitroxides is determined by the static spin-Hamiltonian (\hat{H}):

$$\hat{\rho}(0) = \frac{\exp(-\hat{H}_0/kT)}{\text{Tr}[\exp(-\hat{H}_0/kT)]} \rightarrow \hat{S}_{1z} + \hat{S}_{2z},$$

where the z-axis is chosen to be aligned along the direction of the external magnetic field, and the subscripts number the two electron spins. The arrow points to the relevant portion of $\hat{S}(0)$ assuming a high-temperature approximation. The time evolution of the spin density matrix, $\rho(t)$, is governed by the Liouville–von Neumann equation:

$$\frac{d\hat{\rho}}{dt} = -\frac{i}{\hbar} \hat{H}(t)\hat{\rho}(t) - \hat{\Gamma}(\hat{\rho}(t) - \hat{\rho}(0)).$$

where $\hat{H}\rho \equiv [\hat{H}, \rho]$, \hbar is Plank's constant divided by 2π , $\hat{\Gamma}$ is the relaxation operator, $i^2 = -1$. Neglecting the relaxation, the density matrix evolves under the action of \hat{H} , as:

$$\frac{d\rho}{dt} = -\frac{i}{\hbar} [\hat{H}(t), \rho(t)],$$

the solution of which, after a period of time Δt , yields the density matrix, $\rho(t)$:

$$\rho(t + \Delta t) = e^{-\frac{i\hat{H}\Delta t}{\hbar}} \rho(t) e^{\frac{i\hat{H}\Delta t}{\hbar}} \equiv \hat{U}(\hat{H}, \Delta t)\rho(t) \quad (12.12)$$

Numerical computation using Equation 12.12 of the DQC EPR signal is described below.

The un-normalized relevant part of the initial density matrix for the two coupled nitroxides, with electron spins $S_k = 1/2$, in thermal equilibrium at high temperatures is:

$$\rho(0) \rightarrow S_{1z} + S_{2z} \quad (12.13)$$

(The normalization will be performed at the end of the calculation). The action of the six-pulse DQC sequence is illustrated as follows:

$$\begin{aligned}
 R_1\left(\frac{\pi}{2}\right) &\rightarrow Q_1(t_p) \rightarrow R_2(\pi) \rightarrow Q_2(t_p) \rightarrow R_3\left(\frac{\pi}{2}\right) \rightarrow Q_3(t_{DQ}) \rightarrow R_4(\pi) \rightarrow Q_4(t_{DQ}) \rightarrow \\
 R_5\left(\frac{\pi}{2}\right) &\rightarrow Q_5(t_m - t_p) \rightarrow R_6(\pi) \rightarrow Q_6(t_m - t_p + t_{echo}), \quad (12.14)
 \end{aligned}$$

where R_k ($k = 1, 2, \dots, 6$) are the six pulse propagators, and Q_k ($k = 1, 2, \dots, 6$) are free-evolution propagators. Now, the k th pulse, applied at the time t and acting during the period of time, τ_k , in the frame rotating with the angular frequency of the circular component of microwave magnetic field resonant with Larmor frequency of the nitroxide electron spin, transforms the density matrix, $\rho(t)$, according to:

$$\rho(t) - (R_k) \rightarrow \rho(t + \tau_k) = e^{-i\hat{H}_k\tau_k} \rho(t) e^{i\hat{H}_k\tau_k},$$

with R_k being the k th pulse propagator due to the effective Hamiltonian \hat{H}_k acting during the period of time τ_k . The action of a π -pulse changes the sign of a coherence order, p (defined in Table 12.IV.1 of Appendix 12.IV), and the $\pi/2$ pulse generates other coherence orders so that $p \rightarrow p \pm 1$ (Gemperle *et al.*, 1990). In order to follow the coherence pathways of interest, the density matrix is then projected onto the coherence pathways \mathbf{p}_k , which are chosen after the pulse according to Figure 12.10, as follows:

$$\rho'(t + \tau_k) = P(\mathbf{p}_k)\rho(t + \tau_k), \quad (12.15)$$

where the idempotent operator $P(\mathbf{p}_k)$ projects the density matrix on the coherence pathways \mathbf{p}_k chosen after the k th pulse. As shown in Figure 12.10, the successive coherence pathways of interest are [(1, -1); (-1, 1); (2, -2); (-2, 2); (1); (-1)], that are chosen after the actions of the six pulses, with two branching points that lead to a total of four distinct pathways. The subsequent free evolution during the time t_k transforms $\rho'(t + \tau_k)$ as $\rho'(t + \tau_k) \xrightarrow{Q(t_k)} \rho(t + \tau_k + t_k)$ according to:

$$\rho(t + \tau_k + t_k) = e^{-i\hat{H}_k t_k} \rho'(t + \tau_k) e^{i\hat{H}_k t_k} \quad (12.16)$$

Table 12.IV.1 Coherence pathways and respective matrix elements for two coupled spins.

Coherence order, p	Corresponding matrix elements (i, k) in the electronic subspace of ρ
+2	(1,4)
+1	(1,2), (1,3), (2,4), (3,4)
0	(1,1), (2,2), (2,3), (3,2), (3,3), (4,4)
-1	(2,1), (3,1), (4,2), (4,3)
-2	(4,1)

In Equation 12.16, \hat{H} is the spin-Hamiltonian in the absence of a pulse referred to as \hat{H}_0 below. The density matrix $\rho(t + \tau_k + t_k)$ is next used in place of $\rho(t)$ in Equation 12.15 for the calculation of the density matrix under the action of the $(k + 1)$ -pulse. The steps defined by Equations 12.15 and 12.16 are then repeated to successively transform the density matrix to calculate the final density matrix, which becomes a function of several arguments, $\rho_f = \rho(\boldsymbol{\tau}, \mathbf{t}, \mathbf{p}, t_{\text{echo}}, \eta, \lambda_1, \lambda_2)$. These arguments are defined as follows: $\boldsymbol{\tau} = (\tau_1, \dots, \tau_6)$ are the pulse durations; $\mathbf{t} = (t_1, \dots, t_6)$ are the subsequent free evolution periods; $\mathbf{p} = (\mathbf{p}_1, \dots, \mathbf{p}_6)$ are the relevant coherence orders during the evolution periods; t_k, t_{echo} are time variables used to record the dipolar evolution and to produce the spin echo envelope. The remaining arguments are the Euler angles $\eta = (\chi, \theta, \varphi)$, which define the orientation of the vector \mathbf{r} connecting the magnetic dipoles associated with the electron spins in the laboratory frame (the angle χ was chosen to be zero as the medium is isotropic). In the dipolar (molecular) frame, whose z -axis is coincident with \mathbf{r} , the Euler angles $\lambda_k = (\alpha_k, \beta_k, \gamma_k)$ define the principal axis of the nitroxide magnetic tensors (Figure 12.13) with α_1 chosen to be 0. Finally, the complex echo signal is given by:

$$F_+ = -2\text{Tr}[S_+ \tilde{\rho}_f].$$

where $\tilde{\rho}_f$ is the normalized density matrix.

The various propagators responsible for the evolution of the density matrix, depend on the exact form determined by \hat{H}_0 in the absence of a pulse, or by $\hat{H}_0 + \hat{H}_p$ in the presence of a pulse. Appropriate pulse time intervals τ_k are chosen to achieve nominal flip angles of $\pi/2$ ($k = 1, 3, 5$) and π ($k = 2, 4, 6$), respectively. The various Hamiltonians are:

$$\hat{H}_0 = \hat{H}_{01} + \hat{H}_{02} + \hat{H}_{12} \quad (12.17)$$

with

$$\hat{H}_{0k} = S_{kz} \mathbf{g}_k \cdot \mathbf{B}_0 - \gamma_n I_{kz} B_0 + S_{kz} \mathbf{A}_k \cdot \mathbf{I}_k; \quad (12.18)$$

where $k = 1, 2$ denotes nitroxides 1 and 2, and H_{12} describes their coupling

$$\hat{H}_{12} = \hat{H}_D + \hat{H}_J = \frac{D}{2}(3\cos^2\theta - 1)(S_z^2 - \frac{1}{3}S^2) + J(\frac{1}{2} - 2\mathbf{S}_1 \cdot \mathbf{S}_2). \quad (12.19)$$

Here, J is the electron exchange constant and D is the dipolar coupling constant:

$$D = \frac{3\gamma_e^2 \hbar}{2r^3}, \quad (12.20)$$

which is equivalent to ω_d in eq. 12.4. The dipolar constant $d = 2D/3$ will most often be used throughout the text. In Equation 12.18, $\mathbf{I}_{1,2}$ are the nuclear spins of the nitrogen (^{14}N or ^{15}N) nuclei on the two nitroxides.

The interaction of a nitroxide with the radiation field due to the applied microwave pulse k in the reference frame rotating with the carrier frequency ω_{jf} , usually set at or near the Larmor frequency, is expressed as:

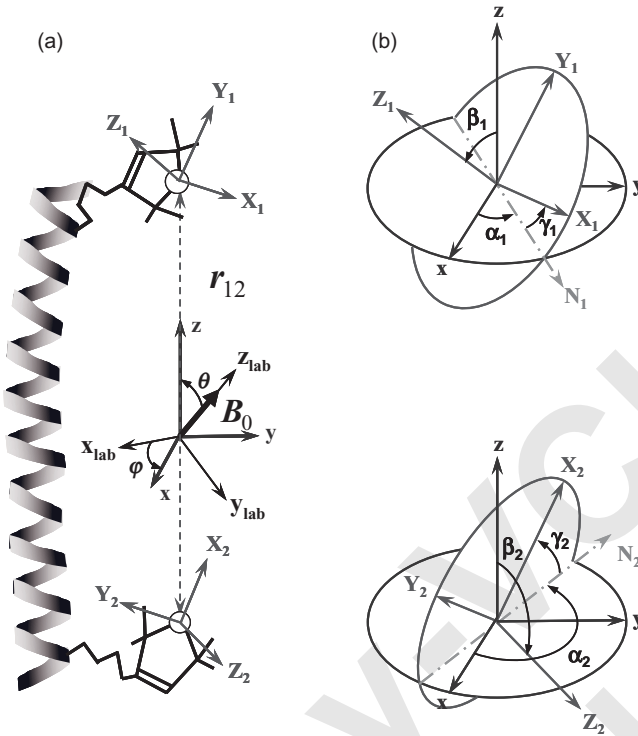


Figure 12.13 The set of Euler angles $\lambda_k = (\alpha_k, \beta_k, \gamma_k)$, ($k = 1, 2$), which define the orientations of the hf and g -tensor principal axes for nitroxides 1 and 2 in the dipolar (reference) frame of reference. In this frame, the z -axis is chosen to coincide with the vector \mathbf{r} , connecting the magnetic dipoles of

the nitroxides. The orientation of the dipolar frame in the laboratory frame (with z -axis parallel to the external magnetic field \mathbf{B}_0) is defined by the Euler angles $\eta = (0, \theta, \varphi)$. Adapted from Misra, Borbat, and Freed (2009).

$$\hat{H}_{pk} = \frac{\gamma_e B_{1k}}{2} (e^{-i\varphi_k} S_+ + e^{i\varphi_k} S_-); \quad (12.21)$$

where B_{1k} is the amplitude of the circular magnetic component. The phases, φ_k , can be set to zero for all the pulses for purposes of the present calculations and consequently $\hat{H}_{pk} = \gamma_e B_{1k} S_x$. The amplitudes, B_{1k} , are assumed to be equal here, but they do not have to be equal for different k -values. \hat{H}_{0k} , as given in Appendix 12.III, describing the spin Hamiltonian for the two nitroxides, becomes in the laboratory frame as

$$\hat{H}_{0k} = C_k S_{kz} + G_k I_{kz} + A_k S_{kz} I_{kz} + B_k S_{kz} I_{k+} + B_k^* S_{kz} I_{k-}$$

The time-domain DQC signal is calculated for a chosen set of λ_k and η , using appropriate variations of the time intervals following the various pulses (as given

in the caption of Figure 12.12 for typical values used for the simulation). The calculations were carried out in the product space $S_1 \otimes S_2 \otimes I_1 \otimes I_2$ with the dimension $N = (2S_1 + 1)(2S_2 + 1)(2I_1 + 1)(2I_2 + 1)$. Accordingly, \hat{H}_0 and \hat{H} are represented by order $N \times N$ matrices \mathbf{H}_0 and \mathbf{H} ; that is, with the size of 36×36 for the two coupled (^{14}N) nitroxides, ($S_{1,2} = 1/2$, $I_{1,2} = 1$). The procedure to calculate $\rho_f(t_{\text{dip}}, t_{\text{echo}}, \theta, \varphi)$ is outlined in Appendix 12.IV.

Finally, the complex echo signal is given by:

$$F_+(t_{\text{dip}}, t_{\text{echo}}, \theta, \phi) = -2\text{Tr}[S_+ \rho_f(t_{\text{dip}}, t_{\text{echo}}, \theta, \varphi)] / \text{Tr}[\mathbf{1}_N].$$

where $\mathbf{1}_N$ is the unit matrix in the product space. For a powder sample, the echo signal is the average of the signals over the orientations of the molecule in the laboratory frame:

$$S(t_{\text{dip}}, t_{\text{echo}}) = \int_0^{2\pi} d\varphi \int_0^\pi F_+(t_{\text{dip}}, t_{\text{echo}}, \theta, \varphi) P_\Omega \sin\theta d\theta. \quad (12.22)$$

In Equation 12.22, P_Ω is the angular distribution of molecular axes in the laboratory frame ($P_\Omega = 1/4\pi$ for an isotropic distribution). In performing powder averaging in isotropic medium, the integration limits to be used are $[0, \pi]$ in axial angles (φ) and $[0, \pi/2]$ in polar angles (θ).

12.6.2

Illustrative Examples

The reader is referred to the publication by Misra, Borbat, and Freed (2009) for a detailed description of the illustrative examples based on the simulation procedure described here. Four of these examples are included in this chapter, as shown in Figures 12.14–12.17, the captions of which provide detailed descriptions.

12.6.3

Conclusions and Future Prospects of Six-Pulse DQC Echo Signal Simulation

The main features and conclusions from the DQC simulations presented here are as follows:

- The simulations for cases of short distances (10–15 Å) are rigorously performed utilizing the full spin Hamiltonian during the pulse.
- The results show that the application of a very strong B_1 field leads to clean Pake doublets in one dimension, that enables one to determine the dipolar (and exchange) couplings with the effects of correlations with the nitroxide magnetic tensors largely suppressed, in most cases. Then, in 2-D format, one may examine the “fingerprint” and make distinctions among different orientations of the principal-axis systems of the magnetic tensors of the nitroxides when correlations are present.
- It is clearly demonstrated from the simulations, that the concept of increased correlation sensitivity in 2-D FT spectra is indeed valid.

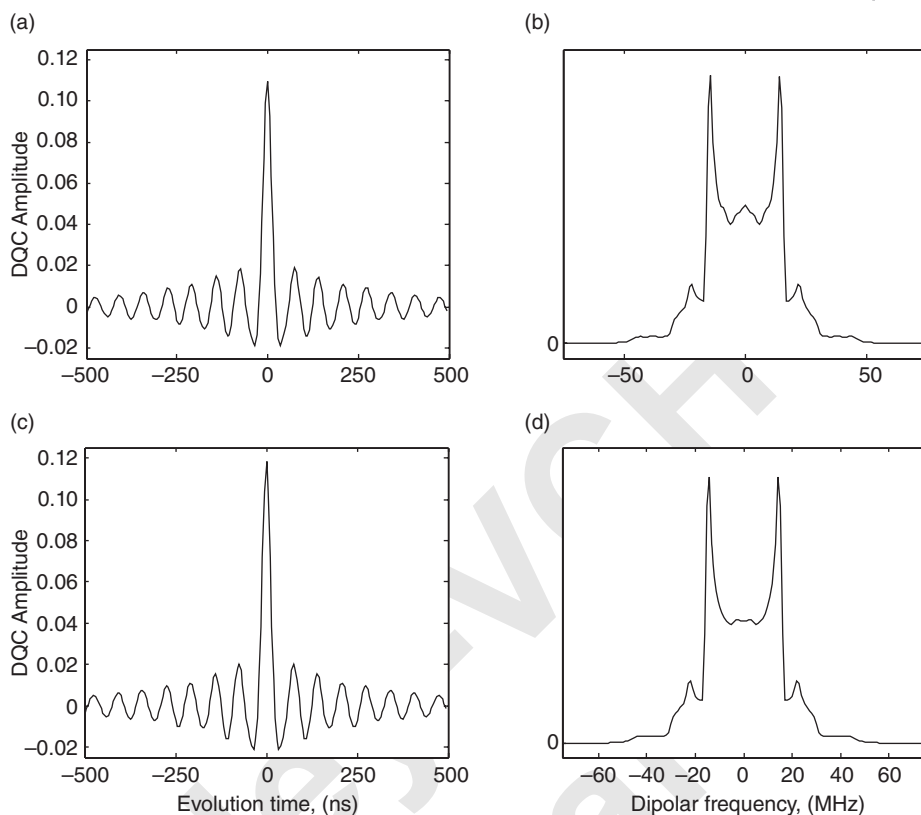


Figure 12.14 (a) Time-domain 1-D DQC signals and their Fourier transforms for ^{14}N nitroxides with their magnetic tensor axes orientations distributed isotropically in the molecular frame (i.e., referred to as uncorrelated case). (Top) – A computation result based on analytical approximation (cf. Equations 12.V.1–12.V.3 in Appendix 12.V) and (bottom) that computed rigorously. $B_0 = 6200\text{ G}$, $B_1 = 30\text{ G}$, and dipolar coupling

(d) is 15 MHz (15.1 \AA). This figure shows the 2-D time-domain data in dipolar and echo times and its 2-D FT. A small peak at $3d/2$ and a weak shoulder extending up to $3d$ are manifestations of the pseudosecular terms in $H_{1,2}$, as given by Equation 12.19. The difference between the two cases is quite small, being mostly caused by using simplified amplitude factors. Adapted from Misra, Borbat, and Freed (2009).

- It is also shown that increased DQC signal strengths are obtained by performing experiments with stronger pulses.
- The criterion for using the approximate analytical approach versus rigorous 1-D simulations at conventional frequencies (up to Q-band) has been established, as discussed in Appendix 12.V.
- For all practical purposes, rigorous DQC simulations should be utilized for the 2-D domain, strong coupling cases, and the millimeter-wave range. Simula-

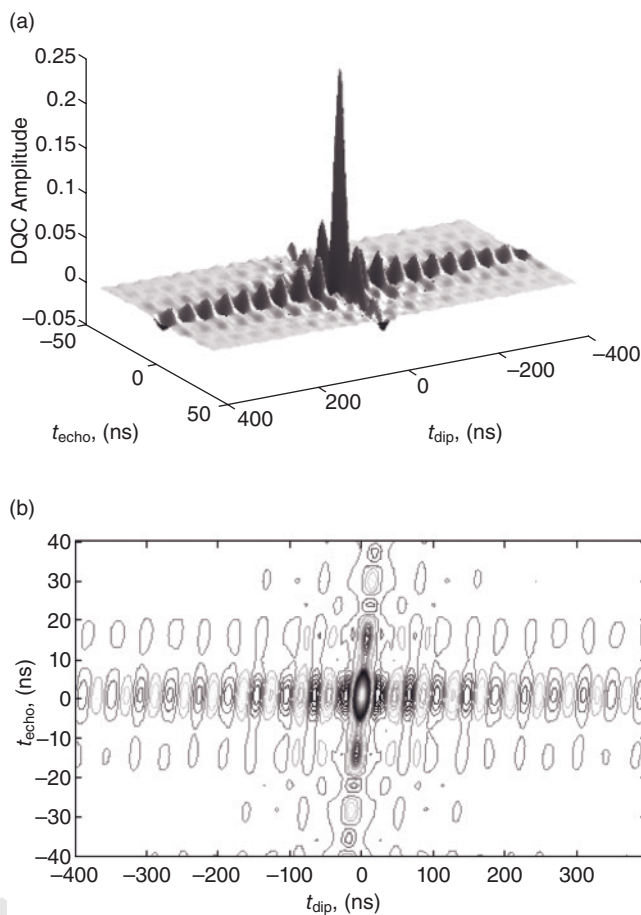


Figure 12.15 Time domain 2-D DQC signal shown as 3-D stack plot and contour plot. The simulations were carried out rigorously for $B_0 = 6200$ G, $B_1 = 60$ G, $d = 25$ MHz and uncorrelated ^{14}N nitroxides. The tilt of the spin-echo refocusing line is clearly visible; this is due to the fact that the spin-echo

envelope is recorded over the time period where only one point corresponds to the dipolar interaction refocusing. A shift by Δt in the spin-echo time corresponds to a shift by $\Delta t/2$ in the position of the dipolar coupling refocusing point. Adapted from Misra, Borbat, and Freed (2009).

tions based on analytic approaches are two to three orders of magnitude computationally more efficient and virtually linearly scalable in multiprocessor-systems. This makes it possible to apply them to more complex cases that include averaging over multiple parameters, data fitting, or to multispin systems.

- The pseudosecular terms exhibit their effects clearly in 1-D and 2-D dipolar data. The pseudosecular part of dipolar coupling is responsible for the spectral

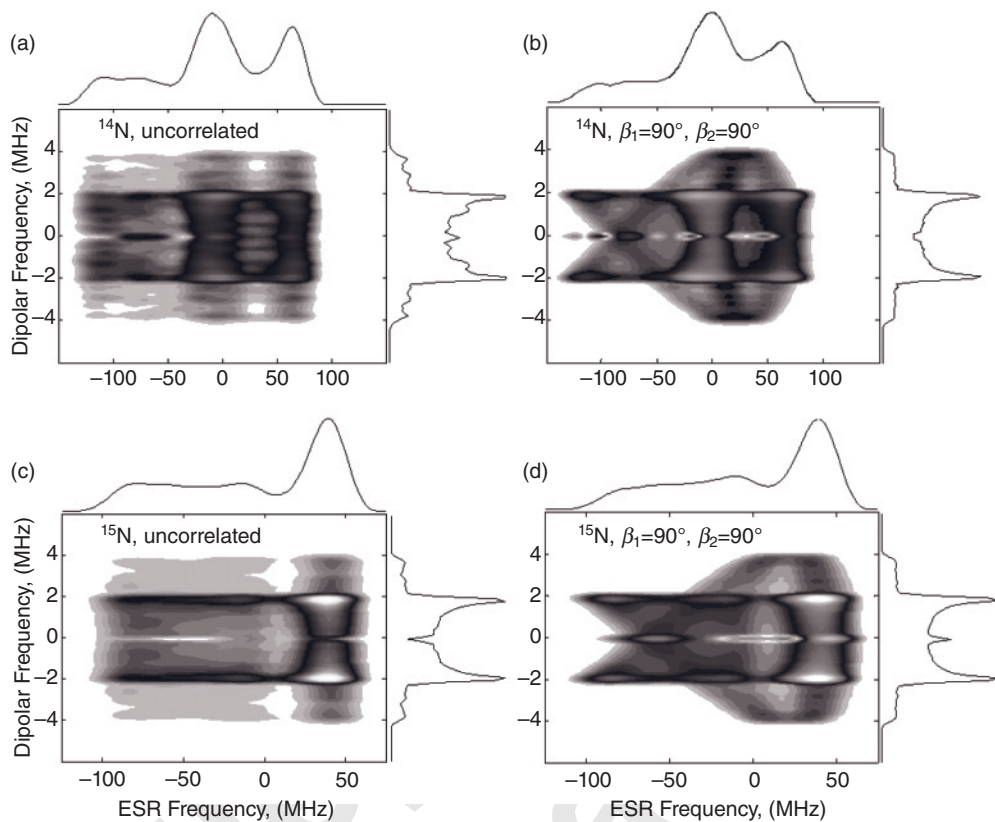


Figure 12.16 2-D DQC (filled) magnitude contour plots obtained by 2-D FT with respect to t_{dip} and t_{echo} . Top row: ^{14}N uncorrelated (a) and correlated (b) case. Bottom row: ^{15}N uncorrelated (c) and correlated (d) cases. $B_0 = 6200\text{G}$, $d = 2\text{MHz}$. B_1 was set to infinity (i.e., perfect pulses), pseudosecular terms were neglected. In (b, d) angles beta were $(90^\circ, 90^\circ)$; the other angles were set to zero. Note the similarity of the 1-D dipolar spectra obtained by integration along the EPR frequency. These

all are classic Pake doublets, but in the 2-D representation the differences are striking. For the uncorrelated cases, the dipolar spectrum is uniform for different slices along the EPR frequency axis, whereas for the correlated case they show a distinct “fingerprint” of this type of correlation. Since pseudosecular terms are neglected, the results are just applicable to long distances, such as the present case. Adapted from Misra, Borbat, and Freed (2009).

peaks with $3d/2$ splitting when two spins resonate at sufficiently close frequencies. This depends differently on orientational correlations than that for the secular part, leading to a richer 2-D spectrum.

- The 1-D spectrum does not show orientational correlations in most cases. On the other hand, the 2-D spectrum does exhibit patterns that are distinct from those obtained in the absence of correlation.

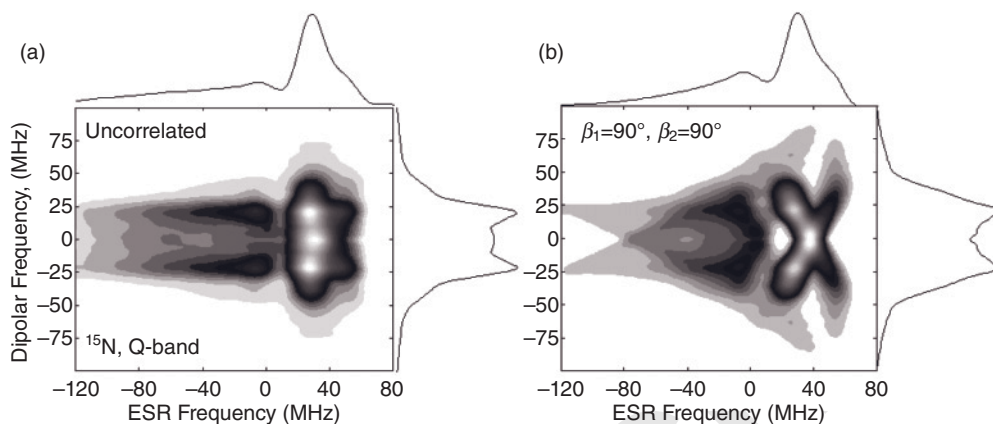


Figure 12.17 2-D DQC (filled) magnitude contour plots computed for ^{15}N nitroxides using $B_0 = 12\,500$, $B_1 = 60$ G, $d = 25$ MHz with a Gaussian distribution in d (FWHM = 5 MHz). Panel (a) represents an uncorrelated case, whereas in (b) the angles beta were $(90^\circ, 90^\circ)$ and alphas and gammas were set to zero. 4×10^4 Monte Carlo trials on a random set in $\{\cos \theta, \varphi, d\}$ were used to generate the data for (a); 180×180 mesh in $\{\cos \theta, \varphi\}$ was used to generate (b). The 1-D dipolar spectra on the right-hand sides of (a, b) are nearly completely smeared, and may

be suited only to estimate d and its variance. The 2-D spectra, however, are quite different. The 2-D spectrum in (b) exhibits a distinct fingerprint of orientational correlation, but the 2-D spectrum for the uncorrelated case in (a) is similar to that in Figure 12.5, in that it tends to streak parallel to EPR frequency axis, as would be expected for such a case, where any point in the EPR spectrum corresponds to all possible orientations. Adapted from Misra, Borbat, and Freed (2009).

- The electron spins are treated here in the point dipole approximation ignoring spin-density delocalization. However, for distances less than about 10 Å, one should take into account spin-density delocalization, which is significant for example, on tyrosyl or flavin radicals, leading to a rhombic dipolar tensor.
- Relaxation effects have not been considered here. Phase relaxation can be introduced phenomenologically, as described by Saxena and Freed (1997) and Borbat and Freed (2000, 2007a), but sufficiently fast spin-lattice relaxation does require treatment with full rigor in Liouville space. However, there exist simplified versions that can be used in Hilbert space (see, for example, Lee, Patyal, and Freed, 1993).

12.7

Sensitivity Considerations: Multifrequency Aspects

The main criterion for sensitivity of PDS (Borbat and Freed, 2000) is based on the ability to measure reliably a distance in a reasonable period of time. An acceptable signal-to-noise ratio (SNR) to this end is nominally taken as a S_{acc} of 10, which

should be attained in an acceptable time of experiment nominally taken as 8 h of signal averaging. However, a S_{acc} of 10 is a bare minimum, and one usually requires a SNR of at least 50 (Chiang, Borbat, and Freed, 2005a). An experimental calibration in the spirit of Borbat and Freed (2000) was made based on a measurement of the spin-echo amplitude using a two-pulse primary echo (PE), which provides the SNR, S_1 (PE), for a single shot. The ratio of the echo amplitudes relevant for DQC versus DEER was ca. 6.5, and the ratio of the SNRs of the single-shot signals at the condition of optimal signal reception was $S_1 \approx 0.42 \mu\text{M}^{-1}$ (DEER) and $S_1 \approx 1.25 \mu\text{M}^{-1}$ (DQC) (for more details, see Borbat and Freed, 2007). Accordingly, the estimates of the dipolar signals for the two techniques are summarized as follows. The S_1 value for DQC, based on a 3/6/3/6/3/6 ns pulse sequence, is greater by a factor of 3.6 than that for a four-pulse DEER with 16/32/32 ns pulses in the detection mode and a 32 ns pump pulse, based on the experimental observations at Cornell. The SNR of the raw data of the full PDS experiment, using the sensitivity analysis given by Borbat and Freed (2000), was estimated to be

$$\text{SNR} = 2S_1 x^2 C \eta_c K(f, T_1) (f t_{\text{exp}}/n)^{1/2} \exp\left(-\frac{2t_{\text{max}}}{T_m} - 2kxCGt_{\text{max}}\right), \quad (12.23)$$

where, t_{max} is the duration of the acquisition of experimental data; f is the frequency of the pulse sequence repetition; n is the number of data points in the record (more details are given by Borbat and Freed, 2000), indicating that Equation 12.23 gives a conservative estimate); C is the concentration of doubly labeled protein (μM); and η_c is the ratio of the sample volume to that used in the calibration. As for the exponential in Equation 12.23, the first term accounts for the phase relaxation, and the second for instantaneous diffusion; G is method specific, which is 0.14 for DEER and ca. 0.52 in DQC; x is the spin-labeling efficiency, which modifies the fraction of both spins that need to be flipped in PDS, exhibiting its strong effect on the outcome of an experiment (assumed to be 1 for complete labeling); $K(f, T_1) = 1 - \exp(-1/fT_1)$ represents the effect of incomplete spin-lattice relaxation for a given relaxation time, T_1 , and the repetition rate, f . The following regimes, supported by experiment, are worthy of note in this context as discussed by Borbat and Freed (2000, 2007).

Short distances, low concentrations: Using Equation 12.23 and the various parameters listed by Borbat and Freed (2000, 2007) for a short distance of 20 Å ($T_{\text{dip}} \equiv v_d^{-1} = 154$ ns), just 4 min of signal averaging of the DQC signal provides a SNR of 10 for a C of 1 μM , whereas DEER will require nearly 60 min to achieve this result. Finally, a high SNR of 100 could be attained for DQC in 6.5 h for the same amount of protein.

Long distances: Using the various parameters listed by Borbat and Freed (2000, 2007) for this case, a SNR of 10 is achieved in 8 h for a C of 2.1 μM for DQC, whereas for DEER one would need 104 h. R_{max} is found to be 59 Å by using one period of T_{dip} , whereas for half of the period, R_{max} is 75 Å. For larger distances, one has a smaller SNR.

Distances in the optimal PDS range: 50 Å is considered to be an upper limit for the “optimal PDS” distance range. Then, T_{dip} is 2.4 μs, for which a t_{max} of 2.4 μs is sufficient to provide the distance reasonably accurately for a structure constraint. For the challenging case of $T_m = 1.5 \mu\text{s}$, a good SNR of 50 is achieved in 16 min by DQC, whereas one requires nearly 3.5 h to achieve the same result by DEER. Shorter distances of 20–45 Å are measured faster, or else yield a better SNR, or better resolution. The spin sensitivity is closely related to the concentration sensitivity, and increases rapidly with an increase in the working frequency due to the small volume of the resonator used at higher frequency. DQC is better suited to handle smaller amounts.

12.7.1

Frequency Dependence of Sensitivity of PDS

The single-shot SNR of the dipolar signal, S_1 , in Equation 12.23 in the absence of relaxation with a view to estimate its frequency dependence is now considered. This is determined by the SNR of the relevant echo signal, which depends on the fraction of the participating *A* spins giving rise to the echo, further modified by a factor (of less than 1) which depends on the fraction of the *B* spins flipped by the pump pulse. (In DQC, the *B* spins are the same as the *A* spins.) A maximum SNR is achieved when nearly all spins are excited, the resonator Q matches the bandwidth of the echo and that of the excitation pulses, and the signal reception is optimized, for example, by matched filtering. As shown by Mims (1965), the single-shot SNR of the part of the echo modified by dipolar coupling, S_1 , is

$$S_1 = \beta_0 \omega C V_s G H (Q \omega / V_c F_N \Delta f)^{1/2}, \quad (12.24)$$

where β_0 is a constant, $\omega = 2\pi f$, with f being the working frequency; C is the spin concentration in the sample; V_c is the resonator effective volume; $V_s = V_c \eta$ is the sample volume, with η being the filling factor of the resonator; G and H are the spectral excitations of spins *A* and *B*, respectively; Q is the loaded Q -value of the resonator; F_N is the system noise figure; and Δf is the receiver bandwidth. A discussion of the typical values of the parameters required in DQC and DEER is given by Borbat and Freed (2000, 2007). Taking all these into account, the SNR that can be achieved for the integrated dipolar signal, turns out to be

$$S_1 \propto \omega^2 C V_c^{1/2} \eta B_s^{-1} K K_2 K_1^{1/2}. \quad (12.25)$$

The frequency dependence of V_c is given by $V_c = \alpha \omega^{-3}$, with α depending on the resonator design, so that the concentration dependence of SNR is

$$S_1(C) \propto C \alpha^{1/2} \omega^{1/2} \eta B_s^{-1} K K_2 K_1^{1/2}. \quad (12.26)$$

On the other hand, the dependence of the absolute sensitivity on the number of spins (N) is

$$S_1(N) \propto N \alpha^{-1/2} \omega^{7/2} B_s^{-1} K K_2 K_1^{1/2}. \quad (12.27)$$

At very high frequencies, for which $B_s^{-1} \propto \omega$, the concentration and spin-number dependencies become

$$S_1(C) \propto C\alpha^{1/2}\omega^{-1/2}\eta KK_2 K_1^{1/2}; \quad (12.28)$$

$$S_1(N) \propto N\alpha^{-1/2}\omega^{5/2}KK_2 K_1^{1/2}. \quad (12.29)$$

Equations 12.28 and 12.29 imply that $S_1(C) \propto \omega^{-1/2}$ and $S_1(N) \propto \omega^{5/2}$, which means that the concentration sensitivity is not significantly benefited by going to higher frequencies, for example, in the millimeter range; however, the absolute sensitivity should be improved. More detailed considerations are required for designing of resonators with a larger value of α .

Recently, Ghimire *et al.* (2009) have found that substantial increase in DEER sensitivity can be obtained by collecting DEER data at Q-band (34 GHz) on a Bruker spectrometer, in comparison with that obtained at X-band (9 GHz) on a Bruker spectrometer. Specifically, in their experiment a 169-fold decrease in data collection time was associated with a huge boost in sensitivity by a factor of 13. They do not fully address instrumental factors responsible for this, nor do they note that the 17 GHz home-made spectrometer of Freed and co-workers has been delivering comparable high sensitivity for a number of years (Borbat and Freed, 2007).

12.8

Distance Distributions: Tikhonov Regularization

In the past, various methods have been proposed to determine the distance distributions of paramagnetic centers in solids (see, for example, Chiang, Borbat, and Freed, 2005a, 2005b; Bowman *et al.*, 2004; and Jeschke *et al.*, 2004). The Tikhonov regularization method (Tikhonov and Arsenin, 1997) has now become routine for extracting distance distributions from the data from both DEER and DQC. It is described as follows.

The time-domain dipolar signal for uniform spin distributions in the sample can be generally expressed as $V_{\text{intra}}A_{\text{inter}} + B_{\text{inter}}$, wherein B_{inter} originates from singly labeled molecules and free label or pairs where one of the spins does not participate. After removing the A and B terms as much as possible, the remainder is a reasonably accurate representation of V_{intra} , which is then subjected to inverse reconstruction by Tikhonov regularization or related methods. One represents the ideal-case problem by a Fredholm integral equation of the first kind

$$V_{\text{intra}}(t) = V_0 \int_0^{\infty} P(r)K(r, t)dr, \quad (12.30)$$

where the kernel $K(r, t)$ for an isotropic sample, using Equations 12.2 and 12.3, is given by

$$K(r, t) = \int_0^1 \cos[\omega_a t(1 - 3x^2)]dx. \quad (12.31)$$

The distance distribution, $P(r)$, is obtained by inversion of the signal V_{intra} , given by Equation 12.30. This can be achieved by using standard numerical methods, such as singular value decomposition (SVD), which in this case is an ill-posed

problem, requiring regularization methods to arrive at a stable solution for $P(r)$. The actual form of the kernel $K(r, t)$ may differ from the ideal form given by Equation 12.31, since the data are discrete and available only over a limited time interval in the practical implementation.

The full distribution in distance, $P(r)$, can be recovered by Tikhonov regularization (Chiang, Borbat, and Freed, 2005a; Chiang, Borbat, and Freed, 2005b; Jeschke *et al.*, 2004). This is accomplished by seeking an optimum $P(r)$, which tries to minimize the residual form of the fit to the data, and at the same time trying to maximize the stability of $P(r)$ by reducing its oscillations. The parameter λ , known as the regularization parameter, determines the relative importance of the two. It is optimized by the L-curve method (Hansen, 1992; Chiang *et al.*, 2005a), which is computationally very efficient and the most reliable available to date. This regularization removes the contributions of the small singular values, σ_i in the SVD that are corrupted by the noise by introducing the filter function:

$$f_i \equiv \frac{\sigma_i^2}{\sigma_i^2 + \lambda^2}, \quad (12.32)$$

which filters out those contributions for which $\sigma_i^2 \ll \lambda^2$. One may then use the maximum-entropy method (MEM) to refine $P(r)$ further, though this computationally more time-consuming (Chiang, Borbat, and Freed, 2005b). One is able to simultaneously fit and remove the effects of A_{inter} and/or B_{inter} while optimizing the $P(r)$ from raw experimental data (Chiang, Borbat, and Freed, 2005a, 2005b) by using the latest versions of MEM and Tikhonov regularization. In this manner, distance distributions are recovered faithfully from the test data, simulated using the ideal kernel of Equation 12.31, even in the presence of significant noise, for example a SNR of 10 (Chiang, Borbat, and Freed, 2005a, 2005b; Bowman *et al.*, 2004; Jeschke *et al.*, 2004). In practice, real data deviate from this ideal picture, and there appears increased uncertainty, which requires a significantly higher SNR.

Recently, Jeschke (2009) has discussed the possibility of overcoming the ill-posed problem of determining distances from DEER data by implementing constraints, such as Tikhonov regularization (Tikhonov, 1955; Jeschke *et al.*, 2004; Chiang, Borbat, and Freed, 2005b). This hides the influence of noise and of other distortions in noise data, and may result in reasonably looking distributions which are actually devoid of any information. Jeschke discusses criteria when DEER data are reliable, as well as a Monte Carlo approach to the validation of distance distributions. Such an approach is achieved by using the software DeerAnalysis2008 (Jeschke *et al.*, 2006; <http://www.epr.ethz.ch/software/index>).

12.9 Additional Technical Aspects of DEER and DQC

Some noteworthy points are summarized as follows (for more details, see Borbat and Freed, 2007, 2007b):

- In the modern approach to PDS, one preferably uses a loop-gap resonators (LGR) or dielectric resonators (DR) to achieve a higher sensitivity, and also a much smaller sample size when required.
- In three-pulse DEER, use of a single amplifier could lead to the problem of not having insufficient power at X-band but was not a problem at Ku-band.
- Since the pulses in four-pulse DEER are not required to be close (unlike those in three-pulse DEER), the significant dead-time effects inherent in three-pulse DEER are avoided in four-pulse DEER, thereby achieving greater sensitivity.
- Although DEER can be used, in principle, without phase cycling or even with incoherent pulses, it is recommended to use spectrometers with high instrument stability, such as are commercially available.
- Suppression of the baseline (background signal) is a key virtue of DQC, and is achieved by extensive phase-cycling, in particular by the use of a double-quantum filter. This diminishes any unwanted modulation of the signal due to low-frequency noise and drifts in phase or gain, as well as nuclear electron spin echo envelope modulation (ESEEM) effects, arising out of modulation of the large background from the single-order coherence signals.
- ESEEM effects: nuclear spin effects are minimized in three-pulse DEER, since the excitation and detections regions are well separated. However, ESEEM effects cannot be neglected in a typical four-pulse DEER experiment with a single power amplifier at X-band. The standard suppression techniques are very successful in both DQC and DEER. In addition, the proton ESEEM is virtually eliminated by increasing the frequency from 9 GHz to 17 GHz, but not the deuterium ESEEM in DQC.
- Orientation selection in DEER and DQC: As discussed by Larsen and Singel (1993) and by Maryasov, Tsvetkov, and Rapp (1998), orientation selection in DEER occurs due to the anisotropy of the nitroxide magnetic tensors, and their orientations relative to the inter-spin vector, which arises out of use of selective pulses. On the other hand, DQC is much less sensitive to orientational selectivity due to use of hard (intense) pulses. If required, however, orientational correlations can be revealed in considerable detail in a 2-D model, as illustrated recently by Misra, Borbat, and Freed (2009). In any case, the flexibility of side-chain labels, such as MTSSL, decreases the correlation effects considerably, whereas at high field it can be exploited to obtain some additional information on orientation of nitroxide side chains, and endogenous radical centers (Denysenkov *et al.*, 2006; Polyhach *et al.*, 2007).

12.10

Concluding Remarks

It has been demonstrated by at Cornell (Borbat *et al.*, 2006; Park *et al.*, 2006; Borbat *et al.*, 2007; Upadhyay *et al.*, 2008; Georgieva *et al.*, 2008; Georgieva *et al.*, 2010; Bhatnagar *et al.*, 2010) as well as in other labs that PDS is clearly capable of being applied to extensive protein mapping. Future developments will enable EPR distance restraints, combined with modeling, nitroxide side-chain geometry simulation, and structure prediction to be applied to identify the detailed 3-D structures of large proteins, and of their complexes. Additional technical improvements are expected in PDS; in particular, DQC has not yet achieved optimum performance, and it is expected that both DQC and DEER will be further developed at a higher frequency. It is hoped that, in the near future, PDS—both as DEER and DQC—will become a standard technique for structural determinations, based on the realization that the technique has many virtues.

Acknowledgments

The authors are very indebted to Peter Borbat for his many seminal contributions to the subjects treated in this chapter and to the many conversations with him about them. S.M. is grateful to Professor C.P. Poole, Jr for constructive comments on this chapter. Partial support for this work is from NIH/NCRR grant # P41-RR016292 (J.H.F.)

Pertinent Literature

The articles by Borbat and Freed (2007a,b) provide an excellent review of PDS, along with a listing of pertinent reports. A recent article by Misra, Borbat, and Freed (2009) treats the simulation of DQC signal on a quantitative basis, the results of which can serve as a standard. The key articles on three-pulse DEER are from Milov, Salikhov, and Shirov (1981) and Larsen and Singel (1993), and the references cited therein. In the case of four-pulse DEER, a key article is that from Pannier *et al.* (2000), and the references cited therein.

References

- | | |
|---|---|
| Banham, J.E., Timmel, C.R., Abbot, R.J.M., Lea, S.M., and Jeschke, G. (2006) <i>Angew. Chem. Int. Ed.</i> , 45 , 1058. | Bhatnagar, J., Borbat, P.P., Pollard, A.M., Freed, J.H., and Crane, B.R. (2010) <i>Biochemistry</i> , 49 , 3824. |
| Bhatnagar, J. (2005) Essay on DEER. Unpublished (Private Communication). For details, contact: skmisra@alcor.concordia.ca. | Borbat, P.P. and Freed, J.H. (1999) <i>Chem. Phys. Lett.</i> , 313 , 145. |
| | Borbat, P.P. and Freed, J.H. (2000) Double-Quantum ESR and distance measurements, |

- in *Biological Magnetic Resonance*, vol. 19 (eds L.J. Berliner, S.S. Eaton, and G.R. Eaton), Kluwer Academic/Plenum Publications, New York, pp. 383–459.
- Borbat, P.P. and Freed, J.H. (2007a) *EPR Newslett.*, **17** (2–3), 21.
- Borbat, P.P. and Freed, J.H. (2007b) *Methods in Enzymology*, **423**, 52.
- Borbat, P.P., Costa-Filho, A.J., Earle, K.A., Moscicki, J.K., and Freed, J.H. (2001) *Science*, **291**, 266.
- Borbat, P.P., Mchaourab, H.S., and Freed, J.H. (2002) *J. Am. Chem. Soc.*, **124**, 5304.
- Borbat, P.P., Davis, J.H., Butcher, S.E., and Freed, J.H. (2004) *J. Am. Chem. Soc.*, **126**, 7746.
- Borbat, P.P., Ramlall, T.F., Freed, J.H., and Eliezer, D. (2006) *J. Am. Chem. Soc.*, **128**, 10004.
- Borbat, P.P., Surendhran, K., Bortolus, M., Zou, P., Freed, J.H., and Mchaourab, H.S. (2007) *PLoS Biology*, **5**, 2211.
- Bowman, M.K., Maryasov, A.G., Kim, N., and DeRose, V.J. (2004) *Appl. Magn. Reson.*, **26**, 223.
- Cai, Q., Kuznetsov, A.K., Hubbell, W.L., Haworth, I.S., Gacho, G.P.C., Eps, N.V., Hideg, K., Chambers, E.J., and Qin, P.Z. (2006) *Nucleic Acids Res.*, **34**, 4722.
- Chiang, Y.-W., Borbat, P.P., and Freed, J.H. (2005a) *J. Magn. Reson.*, **172**, 184.
- Chiang, Y.-W., Borbat, P.P., and Freed, J.H. (2005b) *J. Magn. Reson.*, **172**, 279.
- Denysenkov, V.P., Prisner, T.F., Stubbe, J., and Bennati, M. (2006) *Proc. Natl Acad. Sci. USA*, **103**, 13386.
- Eaton, S.S., More, K.M., Sawant, B.M., and Eaton, G.R. (1983) *J. Am. Chem. Soc.*, **105**, 6560.
- Ernst, R.R., Bodenhausen, G., and Wokaun, A. (1987) *Principles of Nuclear Magnetic Resonance in One and Two Dimensions*, Clarendon Press, Oxford.
- Fafarman, A.T., Borbat, P.P., Freed, J.H., and Kirshenbaum, K. (2007) *Chem. Commun.*, (4), 377.
- Freed, J.H. (1976) The theory of Slow Tumbling ESR Spectra for Nitroxides, in *Spin Labeling: Theory and Application* (ed. L.J. Berliner), Academic Press, New York, Chapter 2, pp. 53–132.
- Freed, J.H. (2000) *Annu. Rev. Phys. Chem.*, **51**, 655.
- Gemperle, C., Aebli, G., Schweiger, A., and Ernst, R.R. (1990) *J. Magn. Reson.*, **88**, 241.
- Gemperle, C., Aebli, G., Schweiger, A., and Hansen, P.C. (1992) *SIAM Rev.*, **34**, 561.
- Georgieva, E.R., Ramlall, T.F., Borbat, P.P., Freed, J.H., and Eliezer, D.J. (2008) *Am. Chem. Soc.* **130**, 12856.
- Georgieva, E.R., Ramlall, T.F., Borbat, P.P., Freed, J.H., and Eliezer, D.J. (2010) *J. Biol. Chem.* **285**, 28261.
- Ghimire, H., McCarrick, R.M., Budil, D.E., and Lorigan, G.A. (2009) *Biochemistry (Rapid Report)*, **48**, 5782.
- Hansen, P.C. (1992) *SIAM Rev.*, **34**, 561.
- Hustedt, E.J., Cobb, C.E., Beth, A.H., and Beechem, J.M. (1993) *Biophys. J.*, **74**, 1861.
- Hustedt, E.J., Smirnov, A.I., Laub, C.F., Cobb, C.E., and Beth, A.H. (1997) *Biophys. J.*, **72**, 1861.
- Jeschke, G. (2002) *Chem. Phys. Chem.*, **3**, 927.
- Jeschke, G. (2009) *EPR Newslett.*, **18**, 15.
- Jeschke, G., Chechlik, V., Ionita, P., Godt, A., Zimmerman, H., Banham, J., Timmel, C.R., Hilger, D., and Jung, H. (2006) *Appl. Magn. Reson.*, **30**, 473.
- Jeschke, G., Pannier, M., and Spiess, H.W. (2000) Double Electron Electron Resonance, in *Biological Magnetic Resonance*, vol. 19 (eds L.J. Berliner, G.R. Eaton, and S.S. Eaton), Plenum, New York, p. 493.
- Jeschke, G., Panek, G., Godt, A., Bender, A., and Paulsen, H. (2004) *Appl. Magn. Reson.*, **26**, 223.
- Klauder, J.R. and Anderson, P.W. (1962) *Phys. Rev.*, **125**, 912.
- Klug, C.S., Camenisch, T.G., Hubbell, W.L., and Hyde, J.S. (2005) *Biophys. J.*, **88**, 3641.
- Kokorin, A.I., Zamarayev, K.I., Grigoryan, G.L., Ivanov, V.P., and Rozantsev, E.G. (1972) *Biofizika*, **17**, 34.
- Larsen, R.G. and Singel, D.J. (1993) *J. Chem. Phys.*, **98**, 5134.
- Lee, S., Patyal, B.R., and Freed, J.H. (1993) *J. Chem. Phys.*, **98**, 3665.
- Lee, S., Budil, D.E., and Freed, J.H. (1994) *J. Chem. Phys.*, **99**, 7098.
- Libertini, L.J., and Griffith, O.H. (1970) *J. Chem. Phys.*, **53**, 1359–1367.
- Martin, R.E., Pannier, M., Diederich, F., Gramlich, V., Hubrich, M., and Spiess, H.W. (1998) *Angew. Chem. Int. Ed.*, **37**, 2834.
- Maryasov, A.G., Tsvetkov, Y.D., and Rapp, J. (1998) *Appl. Magn. Reson.*, **14**, 101.
- Milov, A.D., Salikhov, K.M., and Shirov, M.D. (1981) *Sov. Phys. Solid State*, **23**, 565.

- Milov, A.D., Ponomarev, A.B., and Tsvetkov, Y.D. (1984) *Chem. Phys. Lett.*, **110**, 67.
- Mims, W.B. (1965) *Rev. Sci. Instrum.*, **36**, 1472.
- Misra, S.K. (2007) *J. Magn. Reson.*, **189**, 59.
- Misra, S.K., Borbat, P.P., and Freed, J.H. (2009) *Appl. Magn. Reson.*, **36**, 237.
- Narr, E., Godt, A., and Jeschke, G. (2002) *Angew. Chem. Int. Ed.*, **41**, 3907.
- Pannier, M., Veit, S., Godt, A., Jeschke, G., and Spiess, H.W. (2000) *J. Magn. Reson.*, **142**, 331.
- Park, S.-Y., Borbat, P.P., Gonzalez-Bonet, G., Bhatnagar, J., Pollard, A.M., Freed, J.H., Bilwes, A.M., and Crane, B.R. (2006) *Nat. Struct. Mol. Biol.*, **13**, 400.
- Persson, M., Harbridge, J.R., Hammerstrom, P., Mitri, R., Martensson, L.-G., Carlsson, U., Eaton, G.R., and Eaton, S.S. (2001) *Biophys. J.*, **80**, 2886.
- Polyhach, Y., Godt, A., Bauer, C., and Jeschke, G. (2007) *J. Magn. Reson.*, **185**, 118.
- Press, W.H., Teukolsky, S.A., Vetterling, W.T., and Flannery, B.P. (1992) *Numerical Recipes in Fortran*, 2nd edn, Cambridge University Press, pp. 456–462.
- Rabenstein, M.D. and Shin, Y.-K. (1995) *Proc. Natl Acad. Sci. USA*, **92**, 8239.
- Saxena, S. and Freed, J.H. (1997) *J. Chem. Phys.*, **107**, 1317–1340.
- Schiemann, O., Piton, N., Mu, Y., Stock, G., Engels, J.W., and Prisner, T.F. (2004) *J. Am. Chem. Soc.*, **126**, 5722.
- Schneider, D.J. and Freed, J.H. (1989a) Calculating Slow Motional Magnetic Resonance Spectra: A User's Guide, in *Spin Labeling: Theory and Applications*, Vol. III, Biological Magnetic Resonance 8, (Plenum, NY), pp. 1–76.
- Schneider, D.J. and Freed, J.H. (1989b) Spin Relaxation and Motional Dynamics, in *Advances in Chemical Physics*, vol. 73 (eds J.O. Hirschfelder, R.E. Wyatt, and R.D. Coalson), John Wiley & Sons, Inc., New York, pp. 387–528.
- Sun, J., Voss, J., Hubbell, W.L., and Kaback, H.R. (1999) *Biochemistry*, **38**, 3100.
- Tikhonov, A.N. (1955) *Numerical Methods for the Solution of Ill-Posed Problems*, Kluwer Academic Publishers, Dordrecht, Boston.
- Tikhonov, A.N. and Arsenin, V.Y. (1997) *Solution of Ill-Posed Problems*, Halsted Press, John Wiley & Sons, Inc., New York.
- Upadhyay, A.K., Borbat, P.P., Wang, J., Freed, J.H., and Edmondson, D.E. (2008) *Biochemistry*, **47**, 1554.

Appendix 12.I

Density-Matrix Derivation of Echo Signal for Three-Pulse DEER

Here, calculations are described for a coupled pair of isolated spins in a disordered solid. These calculations are carried out in Hilbert space, wherein the spins are assumed to be quantized along the external magnetic field, B , directed along the Z axis. Relaxation effects are neglected in the present consideration (Bhatnagar, 2005).

The spin Hamiltonian for coupled nitroxides is expressed in frequency units as:

$$H/\hbar = \omega_{01}S_{1z} + \omega_{02}S_{2z} + aS_{1z}S_{2z} \quad (12.I.1)$$

In Equation 12.I.1, $\omega_{01} = \gamma_1 B_0$ is the resonance frequency of the isolated S_1 spins; $\omega_{02} = \gamma_2 B_0$ is the resonance frequency of the isolated S_2 spins; a is the dipolar coupling frequency expressed by Equation 12.2 ignoring the pseudosecular term in Equation 12.1; B_0 is the external magnetic field; and γ_1 , γ_2 are the gyromagnetic ratios for S_1 and S_2 spins, respectively. The following considerations are made in the rotating frame, in which the S_1 spins are off-resonance by ΔB_{01} and the S_2 spins by ΔB_{02} . The corresponding chemical shifts are: $\Delta\omega_{01} = \gamma_1 \Delta B_{01} - \omega_{01}$ and $\Delta\omega_{02} = \gamma_2 \Delta B_{02} - \omega_{02}$.

The pulse sequence in three-pulse DEER is: $X_1(\pi/2) \text{ --- } \tau \text{ --- } X_S(\pi/2) \text{ --- } (\tau' - \tau) \text{ --- } X_1(\pi) \text{ --- } (t - \tau')$. In other words, at the time $t = 0^-$, a $\pi/2$ pulse, $X_1(\pi/2)$,

is applied on S_1 spins about the X axis. Thereafter, at time τ , a $\pi/2$, $X_2(\pi/2)$, pulse is applied on S_2 spins about the X -axis, followed by the application of a π -pulse on S_1 spins about the X axis, $X_1(\pi)$, after a time delay of $(\tau - \tau')$. The subsequent time evolution of the density matrix for $t > \tau'$ produces an echo for S_1 spins at $t = 2\tau'$, which is the signal of interest here.

The echo signal for S_1 spins at any time is given by the expectation value of the transverse magnetization, proportional to $\langle S_1^+(t) \rangle = \text{Tr}\{S_1^+\rho(t)\}$, where Tr stands for trace. The initial value of the density matrix, considering the Zeeman terms only, ignoring the dipolar and exchange terms, is:

$$\rho(0^-) = \exp(-H/k_B T)/Z \approx \{1 - (\hbar\omega_{01}S_{1z} + \hbar\omega_{02}S_{2z})/k_B T\}/Z, \quad (12.1.2)$$

where $Z = 1/\sum_i \exp(-E_i/k_B T)$, the sum being over the four energy states of the two coupled nitroxides with spin $1/2$ each; T is the temperature; and k_B is the Boltzmann constant.

The $\pi/2$ pulse, applied on S_1 spins about the X -axis at $t = 0^-$, transforms the density matrix to:

$$\begin{aligned} \rho(0^+) &= X_1(\pi/2)\rho(0^-)X_1^{-1}(\pi/2) \\ &= X_1(\pi/2)(1/Z)\{1 - (\hbar\omega_{01}S_{1z} + \hbar\omega_{02}S_{2z})/k_B T\}X_1^{-1}(\pi/2) \end{aligned} \quad (12.1.3)$$

where $X_1(\pi/2) = e^{i\frac{\pi}{2}S_{1x}}$. The $X_1(\pi/2)$ pulse rotates the S_1 magnetization from the Z axis to Y axis, and has no effect on S_2 spins: $e^{i\frac{\pi}{2}S_{1x}}S_{1z}e^{-i\frac{\pi}{2}S_{1x}} = S_{1y}$.

Now, since only the echo signal from S_1 spins is detected, the constant term and the term in S_{2z} in the initial value of the density matrix does not contribute to it, so they are hereafter ignored in the density matrix. Thus, considering only the term with S_{1y} , one has

$$\rho(0^+) = -\hbar\omega_{01}S_{1y}/(Zk_B T) \quad (12.1.4)$$

The evolution of the density matrix under the effect of the static Hamiltonian,

$$H_s = \Delta\omega_1S_{1z} + \Delta\omega_2S_{2z} - aS_{1z}S_{2z} \quad (12.1.5)$$

over the time interval τ is now considered for $0 < t < \tau$:

$$\rho(t) = e^{i(\Delta\omega_1S_{1z} + \Delta\omega_2S_{2z} - aS_{1z}S_{2z})t} \rho(0^+) e^{-i(\Delta\omega_1S_{1z} + \Delta\omega_2S_{2z} - aS_{1z}S_{2z})t} \quad (12.1.6)$$

After the application of a π -pulse about the X -axis on S_2 spins at $t = \tau^-$, one obtains from Equations 12.1.4 and 12.1.5 the resulting density matrix:

$$\begin{aligned} \rho(\tau^+) &= X_2(\pi)\rho(\tau^-)X_2^{-1}(\pi) \\ &= (-\hbar\omega_{01}/Zk_B T)X_2(\pi)e^{i(\Delta\omega_1S_{1z} + \Delta\omega_2S_{2z} - aS_{1z}S_{2z})\tau}S_{1y}e^{-i(\Delta\omega_1S_{1z} + \Delta\omega_2S_{2z} - aS_{1z}S_{2z})\tau}X_2^{-1}(\pi) \end{aligned} \quad (12.1.7)$$

Inserting the unit operator $(X_2^{-1}(\pi)X_2(\pi))$ in Equation 12.1.7 before and after S_{1y} , and writing it as a product of three terms, one obtains:

$$\rho(\tau^+) = (-\hbar\omega_{01}/Zk_B T)A^*B^*C,$$

where $A = X_2(\pi)e^{i(\Delta\omega_1S_{1z} + \Delta\omega_2S_{2z} - aS_{1z}S_{2z})\tau}X_2^{-1}(\pi)$; $B = X_2(\pi)S_{1y}X_2^{-1}(\pi)$; and $C = X_2(\pi)e^{-i(\Delta\omega_1S_{1z} + \Delta\omega_2S_{2z} - aS_{1z}S_{2z})\tau}X_2^{-1}(\pi)$.

Now, since the S_1 and S_2 operators commute, the B -term simply reduces to S_{1y} . As for the terms A and C , the $X_2(\pi)$ pulse will simply reverse the signs of the exponentials of the terms $e^{i\Delta\omega_2S_{2z}}$ and $e^{-iaS_{1z}S_{2z}}$, while leaving $e^{i\Delta\omega_1S_{1z}}$ unchanged, since the pulse is selective to S_2 spins only, so that $A = e^{i(\Delta\omega_1S_{1z} - \Delta\omega_2S_{2z} + aS_{1z}S_{2z})\tau}$ and $C = e^{-i(\Delta\omega_1S_{1z} - \Delta\omega_2S_{2z} + aS_{1z}S_{2z})\tau}$. One, therefore, obtains for the density matrix after the application of the $X_2(\pi)$ pulse at $t = \tau^-$

$$\rho(\tau^+) = (-\hbar\omega/Zk_B T)e^{i(\Delta\omega_1S_{1z} - \Delta\omega_2S_{2z} + aS_{1z}S_{2z})\tau}S_{1y}e^{-i(\Delta\omega_1S_{1z} - \Delta\omega_2S_{2z} + aS_{1z}S_{2z})\tau} \quad (12.I.8)$$

Since the operators S_1 and S_2 commute, the above expression can be simplified by putting the terms containing only the S_{2z} operators in the exponentials on the left and right sides of S_{1y} equal to zero. Then, one obtains

$$\rho(\tau^+) = (-\hbar\omega_{01}/Zk_B T)e^{i(\Delta\omega_1S_{1z} + aS_{1z}S_{2z})\tau}S_{1y}e^{-i(\Delta\omega_1S_{1z} + aS_{1z}S_{2z})\tau} \quad (12.I.9)$$

Now, the system evolves during the time $(\tau' - \tau)$ before a π -pulse is applied to S_1 spins, that is for $\tau < t < \tau'$, during which the density matrix evolves under the action of the static Hamiltonian H_s :

$$\rho(t) = e^{i(\Delta\omega_1S_{1z} + \Delta\omega_2S_{2z} - aS_{1z}S_{2z})(t - \tau)}\rho(\tau^+)e^{-i(\Delta\omega_1S_{1z} + \Delta\omega_2S_{2z} - aS_{1z}S_{2z})(t - \tau)} \quad (12.I.10)$$

Using the expression for $\rho(\tau^+)$ from Equation 12.I.9, one obtains for the density matrix at $t = \tau'^-$,

$$\rho(\tau'^-) = (-\hbar\omega_{01}/Zk_B T)e^{i\Delta\omega_1S_{1z}\tau'}e^{-iaS_{1z}S_{2z}(\tau' - 2\tau)}S_{1y}e^{-i\Delta\omega_1S_{1z}\tau'}e^{-i\Delta\omega}e^{iaS_{1z}S_{2z}(\tau' - 2\tau)} \quad (12.I.11)$$

In simplifying Equation 12.I.11 it is noted that, after substituting the expression for $\rho(\tau^+)$ from Equation 12.I.9, the terms involving $e^{i\Delta\omega_2S_{2z}(\tau' - 2\tau)}$ on the left of S_{1y} and $e^{-i\Delta\omega_2S_{2z}(\tau' - 2\tau)}$ on the right side cancel out, since S_{1y} and S_{2z} commute with each other.

Now, at $t = \tau'^-$, the application of a π -pulse to S_1 spins about the X -axis transforms it according to:

$$\begin{aligned} \rho(\tau'^+) &= X_1(\pi)\rho(\tau'^-)X_1^{-1}(\pi) = X_1(\pi)(-\hbar\omega_{01}/Zk_B T)e^{i\Delta\omega_1S_{1z}\tau'}e^{-iaS_{1z}S_{2z}(\tau' - 2\tau)} \\ &S_{1y}e^{-i\Delta\omega_1S_{1z}\tau'}e^{iaS_{1z}S_{2z}(\tau' - 2\tau)}X_1^{-1}(\pi) \end{aligned} \quad (12.I.12)$$

Now, by inserting the unity operator $[= X_1(\pi)X_1^{-1}(\pi)]$ twice on the right-hand side of the above equation, and using the same procedure as that used to derive Equation 12.I.8 for $\rho(\tau^+)$, one obtains

$$\begin{aligned} \rho(\tau'^+) &= (-\hbar\omega_{01}/Zk_B T)A^*B^*C, \text{ where} \\ A &= X_1(\pi)e^{i\Delta\omega_1S_{1z}\tau'}e^{-iaS_{1z}S_{2z}(\tau' - 2\tau)}X_1^{-1}(\pi) = e^{-i\Delta\omega_1S_{1z}\tau'}e^{iaS_{1z}S_{2z}(\tau' - 2\tau)}, \\ B &= X_1(\pi)S_{1y}X_1^{-1}(\pi) = -S_{1y}; \text{ and} \\ C &= X_1(\pi)e^{-i\Delta\omega_1S_{1z}\tau'}e^{iaS_{1z}S_{2z}(\tau' - 2\tau)}X_1^{-1}(\pi) = e^{i\Delta\omega_1S_{1z}\tau'}e^{-iaS_{1z}S_{2z}(\tau' - 2\tau)} \end{aligned}$$

In simplifying B to the second term on the right in the above equation, the fact that a rotation by 180° about the X -axis will orient the magnetization of S_1 spins

along the negative Y axis has been taken into account. Further, as for simplifications of the terms A and C , the selective X_1 π -pulse for S_1 spins will reverse the orientations of S_1 spins. This will result in reversals of the signs of the exponents of $e^{i\Delta\omega_1 S_{1z}\tau'}$ and $e^{-iaS_{1z}S_{2z}(\tau'-2\tau)}$ in the A term, and those of $e^{-i\Delta\omega_1 S_{1z}\tau'}$ and $e^{iaS_{1z}S_{2z}(\tau'-2\tau)}$ in the C term. Finally,

$$\rho(\tau'^+) = (\hbar\omega_{01}/Zk_B T) e^{-i\Delta\omega_1 S_{1z}\tau'} e^{iaS_{1z}S_{2z}(\tau'-2\tau)} S_{1y} e^{i\Delta\omega_1 S_{1z}\tau'} e^{-iaS_{1z}S_{2z}(\tau'-2\tau)} \quad (12.I.13)$$

Now, the system evolves under the action of the static Hamiltonian for time $t > \tau'$, during which

$$\rho(t) = e^{i(\Delta\omega_1 S_{1z} + \Delta\omega_2 S_{2z} - aS_{1z}S_{2z})(t-\tau')} \rho(\tau'^+) e^{-i(\Delta\omega_1 S_{1z} + \Delta\omega_2 S_{2z} - aS_{1z}S_{2z})(t-\tau')} \quad (12.I.14)$$

By substituting Equation 12.I.13 for $\rho(\tau'^+)$ in Equation 12.I.14, and simplifying, one obtains

$$\rho(t) = (\hbar\omega_{01}/Zk_B T) e^{i\Delta\omega_1 S_{1z}(t-2\tau')} e^{-iaS_{1z}S_{2z}(t+2\tau-2\tau')} S_{1y} e^{-i\Delta\omega_1 S_{1z}(t-2\tau')} e^{iaS_{1z}S_{2z}(t+2\tau-2\tau')} \quad (12.I.15)$$

At the time $t = 2\tau'$, when the echo is formed, the exponentials involving $\Delta\omega_1$ simplify to unity, leaving only the terms with $S_{1z}S_{2z}$. Then the density matrix becomes

$$\rho(2\tau') = (\hbar\omega_{01}/Zk_B T) e^{iaS_{1z}S_{2z}2\tau} S_{1y} e^{-iaS_{1z}S_{2z}2\tau} \quad (12.I.16)$$

The echo amplitude at the time $t = 2\tau'$ will then be

$$\langle S_1^+(2\tau') \rangle = \text{Tr}\{S_1^+ \rho(2\tau')\} = (\hbar\omega_{01}/Zk_B T) \text{Tr}\{S_1^+ e^{iaS_{1z}S_{2z}2\tau} S_{1y} e^{-iaS_{1z}S_{2z}2\tau}\} \quad (12.I.17)$$

The term in the curly brackets in Equation 12.I.17 depends on the spin-spin coupling only, since the effects of the chemical shifts and field inhomogeneities have been canceled out due to refocusing, and do not affect the magnetization (echo) at $t = 2\tau'$.

For a system consisting of two spin $-1/2$, S_1 and S_2 , the operator for the magnetization of spins S_1 is proportional to $S_1^+ 1_2$, where $S_1^+ = S_{1x} + iS_{1y}$ and 1_2 is the unit operator in the space of S_2 . In order to evaluate the trace in Equation 12.I.17, using the direct-product space of spins S_1 and S_2 , one obtains

$$\begin{aligned} & \text{Tr}\{(S_1^+ 1_2) e^{iaS_{1z}S_{2z}2\tau} (S_{1y} 1_2) e^{-iaS_{1z}S_{2z}2\tau}\} \\ &= \sum_{M_1 M_2} \langle M_1 M_2 | (S_1^+ 1_2) e^{iaS_{1z}S_{2z}2\tau} (S_{1y} 1_2) e^{-iaS_{1z}S_{2z}2\tau} | M_1 M_2 \rangle \\ &= \sum_{M_2} \langle 1/2 M_2 | S_1^+ 1_2 | -1/2 M_2 \rangle e^{-iaM_2\tau} \langle -1/2 M_2 | \frac{i}{2} S_1^- 1_2 | 1/2 M_2 \rangle e^{-iaM_2\tau} \\ &= \frac{i}{2} (e^{ia\tau} + e^{-ia\tau}) = i \cos(a\tau) \end{aligned} \quad (12.I.18)$$

In Equation 12.I.18 $M_1 (= \pm 1/2)$ and $M_2 (= \pm 1/2)$ are the electronic spin magnetic quantum numbers for spins S_1 and S_2 , respectively. The third line in Equation 12.I.18 is obtained from the preceding line by: (i) introducing the unity operators

$$\sum_{M_1' M_2'} |M_1' M_2'\rangle \langle M_1' M_2'| = 1, \quad \sum_{M_1'' M_2''} |M_1'' M_2''\rangle \langle M_1'' M_2''| = 1, \quad \text{and} \quad \sum_{M_1''' M_2'''} |M_1''' M_2'''\rangle \langle M_1''' M_2'''| = 1$$

the operator S_1^+ , before and after the operator S_{1y} , respectively; and (ii) taking into account the nonzero matrix elements of the operators in the S_1 space, specifically $\langle M_1 = 1/2 | S_1^+ | M_1 = -1/2 \rangle = \langle M_1 = -1/2 | S_1^- | M_1 = 1/2 \rangle = 1$ and $\langle M_2 = 1/2 | S_{2z} | M_2 = 1/2 \rangle = -\langle M_2 = -1/2 | S_{2z} | M_2 = -1/2 \rangle = 1/2$, and (iii) $S_{1y} = (S_1^+ - S_1^-)/2i$.

Finally, one obtains from Equation 12.I.17

$$\langle S_1^+(2\tau') \rangle = i[\hbar\omega_{01} \cos(a\tau)/Zk_B T] = iI_0 \cos(a\tau), \quad (12.I.19)$$

where $I_0 = \hbar\omega_{01}/Zk_B T$.

Equation 12.I.19 shows that the imaginary part of the echo amplitude of three-pulse DEER at $t = 2\tau'$ is modulated by the factor $\cos(a\tau)$.

Appendix 12.II

Density-Matrix Derivation of the Echo Signal for Four-Pulse DEER

Schematically, the Four-pulse sequence can be written in the following form:

$$X_1(\pi/2) - \tau_1 - X_1(\pi) - t - X_S(\pi) - (\tau_1 + \tau_2 - t) - X_1(\pi) - (t' - 2\tau_1 - \tau_2).$$

In order to find out the form of the detected signal, as mentioned before, one needs to calculate $\langle S_1^+(2\tau_1 + 2\tau_2) \rangle$. A procedure similar to that used with three-pulse sequence in Appendix 12.I will be followed here (Bhatnagar, 2005). Accordingly, the initial density matrix, in the high-temperature approximation, is

$$\rho(0^-) \approx \{1 - (\hbar\omega_{01}S_{1z} - \hbar\omega_{02}S_{2z})/k_B T\}/Z \quad (12.II.1)$$

and

$$\rho(0^+) \approx -\hbar\omega_{01}S_{1y}/(Zk_B T) \quad (12.II.2)$$

Now, the system evolves under the action of the static Hamiltonian, given by Equation 12.I.5 for a time τ_1 after which a S_1 -selective π pulse is applied about the X axis. For $0 < t' < \tau_1$,

$$\rho(t') = e^{i(\Delta\omega_1 S_{1z} + \Delta\omega_2 S_{2z} - aS_{1z} S_{2z})t'} \rho(0^+) e^{-i(\Delta\omega_1 S_{1z} + \Delta\omega_2 S_{2z} - aS_{1z} S_{2z})t'} \quad (12.II.3)$$

After a π pulse is applied on S_1 spins at $t = \tau_1^-$, one obtains

$$\begin{aligned} \rho(\tau_1^+) &= X_1(\pi)\rho(\tau_1^-)X_1^{-1}(\pi) \\ &= (-\hbar\omega_{01}/Zk_B T)X_1(\pi)e^{i(\Delta\omega_1 S_{1z} + \Delta\omega_2 S_{2z} - aS_{1z} S_{2z})\tau_1} S_{1y} e^{-i(\Delta\omega_1 S_{1z} + \Delta\omega_2 S_{2z} - aS_{1z} S_{2z})\tau_1} X_1^{-1}(\pi) \end{aligned} \quad (12.II.4)$$

Inserting the unit operator ($X_1^{-1}(\pi)X_1(\pi)$) in Equation 12.II.4 before and after S_{1y} , and writing it as a product of three terms, following the same procedure as that used in Appendix 12.I after Equation 12.I.7, one obtains:

$$\rho(\tau_1^+) = (-\hbar\omega_{01}/Zk_B T) e^{-i(\Delta\omega_1 S_{1z} - \Delta\omega_2 S_{2z} - aS_{1z} S_{2z})\tau_1} (-S_{1y}) e^{i(\Delta\omega_1 S_{1z} - \Delta\omega_2 S_{2z} - aS_{1z} S_{2z})\tau_1} \quad (12.II.5)$$

Now, the system evolves for time t , after which a π pulse is applied on S_2 spins. During this time, $\tau_1 < t' < \tau_1 + t$, one obtains:

$$\rho(t') = e^{i(\Delta\omega_1 S_{1z} + \Delta\omega_2 S_{2z} - a S_{1z} S_{2z})(t' - \tau_1)} \rho(\tau_1^+) e^{-i(\Delta\omega_1 S_{1z} + \Delta\omega_2 S_{2z} - a S_{1z} S_{2z})(t' - \tau_1)} \quad (12.II.6)$$

Substituting now $t' = \tau_1 + t$, one obtains from Equation 12.II.6

$$\rho(\tau_1 + t^-) = (-\hbar\omega_{01}/Zk_B T) e^{i(\Delta\omega_1 S_{1z} - a S_{1z} S_{2z})(t - \tau_1)} (-S_{1y}) e^{-i(\Delta\omega_1 S_{1z} - a S_{1z} S_{2z})(t - \tau_1)} \quad (12.II.7)$$

In writing the above expression, the terms with $\Delta\omega_2 S_{2z}$ have been canceled out since S_{2z} commutes with S_{1y} .

Now a π pulse is applied to S_2 spins, which transforms the density matrix to

$$\begin{aligned} \rho(\tau_1 + t^+) &= X_2(\pi) \rho(\tau_1 + t^-) X_2^{-1}(\pi) \\ &= (-\hbar\omega_{01}/Zk_B T) X_2(\pi) e^{i(\Delta\omega_1 S_{1z} - a S_{1z} S_{2z})(t - \tau_1)} (-S_{1y}) e^{-i(\Delta\omega_1 S_{1z} - a S_{1z} S_{2z})(t - \tau_1)} X_2^{-1}(\pi) \end{aligned} \quad (12.II.8)$$

Inserting now the unit operator ($X_2^{-1}(\pi)X_2(\pi)$) in Equation 12.II.8 before and after S_{1y} , and writing it as a product of three terms, following the same procedure as that used in Appendix 12.I after Equation 12.9, one obtains:

$$\rho(\tau_1 + t^+) = (-\hbar\omega_{01}/Zk_B T) e^{i(\Delta\omega_1 S_{1z} + a S_{1z} S_{2z})(t - \tau_1)} (-S_{1y}) e^{-i(\Delta\omega_1 S_{1z} + a S_{1z} S_{2z})(t - \tau_1)} \quad (12.II.9)$$

Subsequent to this, the system evolves under the action of static Hamiltonian during the period $(\tau_1 + \tau_2 - t)$. Then, one can express for $\tau_1 + t < t' < 2\tau_1 + \tau_2$:

$$\rho(t') = e^{i(\Delta\omega_1 S_{1z} + \Delta\omega_2 S_{2z} - a S_{1z} S_{2z})(t' - \tau_1 - t)} \rho(\tau_1 + t^+) e^{-i(\Delta\omega_1 S_{1z} + \Delta\omega_2 S_{2z} - a S_{1z} S_{2z})(t' - \tau_1 - t)} \quad (12.II.10)$$

From Equation 12.II.10 at $t' = 2\tau_1 + \tau_2$, one obtains

$$\rho(2\tau_1 + \tau_2^-) = e^{i(\Delta\omega_1 S_{1z} + \Delta\omega_2 S_{2z} - a S_{1z} S_{2z})(\tau_2 + \tau_1 - t)} \rho(\tau_1 + t^+) e^{-i(\Delta\omega_1 S_{1z} + \Delta\omega_2 S_{2z} - a S_{1z} S_{2z})(\tau_2 + \tau_1 - t)} \quad (12.II.11)$$

Substituting now $\rho(\tau_1 + t^+)$ from Equation 12.II.9, one obtains

$$\rho(2\tau_1 + \tau_2^-) = (-\hbar\omega_{01}/Zk_B T) e^{i\Delta\omega_1 S_{1z} \tau_2} e^{ia S_{1z} S_{2z} (2\tau_1 - 2\tau_1 - \tau_2)} (-S_{1y}) e^{-i\Delta\omega_1 S_{1z} \tau_2} e^{-ia S_{1z} S_{2z} (2\tau_1 - 2\tau_1 - \tau_2)} \quad (12.II.12)$$

An S_1 -selective π pulse is now applied at $t' = 2\tau_1 + \tau_2$, which yields:

$$\rho(2\tau_1 + \tau_2^+) = X_1(\pi) \rho(2\tau_1 + \tau_2^-) X_1^{-1}(\pi) \quad (12.II.13)$$

Inserting now the unit operator ($X_1^{-1}(\pi)X_1(\pi)$) in Equation 12.II.9 before and after S_{1y} , and writing it as a product of three terms, following the same procedure as that used in Appendix 12.I after Equation 12.I.7, one obtains:

$$\rho(2\tau_1 + \tau_2^+) = e^{-i\Delta\omega_1 S_{1z} \tau_2} e^{-ia S_{1z} S_{2z} (2\tau_1 - 2\tau_1 - \tau_2)} S_{1y} e^{i\Delta\omega_1 S_{1z} \tau_2} e^{ia S_{1z} S_{2z} (2\tau_1 - 2\tau_1 - \tau_2)} \quad (12.II.14)$$

The system now evolves under the action of the static Hamiltonian. One obtains for the density matrix for the time $t' > 2\tau_1 + \tau_2$:

$$\rho(t') = e^{i(\Delta\omega_1 S_{1z} + \Delta\omega_2 S_{2z} - ia S_{1z} S_{2z})(t' - 2\tau_1 - \tau_2)} \rho(2\tau_1 + \tau_2^+) e^{-i(\Delta\omega_1 S_{1z} + \Delta\omega_2 S_{2z} - ia S_{1z} S_{2z})(t' - 2\tau_1 - \tau_2)} \quad (12.II.15)$$

After calculating the density matrix at $t' = 2\tau_1 + 2\tau_2$ and substituting the value of $\rho(2\tau_1 + \tau_2^+)$ from Equation 12.II.14, one obtains the following expression:

$$\rho(2\tau_1 + 2\tau_2) = (-\hbar\omega_{01}/Zk_B T) e^{-iaS_{1z}S_{2z}(2t-2\tau_1)} S_{1y} e^{iaS_{1z}S_{2z}(2t-2\tau_1)} \quad (12.II.16)$$

In order to calculate $\langle S_1^+(2\tau_1 + 2\tau_2) \rangle$, the echo due to the four-pulse sequence, one proceeds in the same way as that for a three-pulse DEER sequence, obtaining

$$\langle S_1^+(2\tau_1 + 2\tau_2) \rangle = -iI_0 \cos(a[t - \tau_1]) = -iI_0 \cos[\omega_{ec}(t - \tau_1)], \quad (12.II.17)$$

where $I_0 = \hbar\omega_{01}/(Zk_B T)$.

Appendix 12.III

Spin Hamiltonian for Coupled Nitroxides Used in Six-Pulse DQC Calculation

One can express the Zeeman and hyperfine part of the nitroxide spin Hamiltonian, H_0 , in the irreducible spherical tensor operator (ISTO) representation (Freed, 1976; Schneider and Freed, 1989a,b; Misra, 2007) as follows:

$$H_0 = \sum_{\mu_k, L, M} F_{\mu_k, \ell}^{L, M*} A_{\mu_k, \ell}^{L, M},$$

where L is the tensor rank (0 or 2); $M = -L, \dots, L$; $k = 1, 2$ numbers the nitroxides; and ℓ denotes the reference frame where the tensors are defined, that is, magnetic frame (g_k), molecular (dipolar) frame (d), or laboratory frame (l). $A_{\mu_k, \ell}^{L, M}$ are the spin operators with μ_k referring to the kind of magnetic interaction, electron Zeeman (g), nuclear Zeeman (N), or hyperfine (A), and they are usually defined in the laboratory frame, $F_{\mu_j, \ell}^{L, M}$ is proportional to the ISTO of the magnetic interaction and is most conveniently defined in the g -frame. The transformation of $F_{\mu_k, gk}^{L, M}$ to the laboratory frame yields the H_0 . In the high-field limit, where the non-secular terms ($S_{\pm}, S_{\pm}I_z, S_{\pm}I_{\pm}, S_{\pm}I_{\mp}$) can be omitted, the ISTO form of the g -tensor reduces to:

$$\begin{aligned} F_{gk, gk}^{0,0} &= -\sqrt{\frac{1}{3}} \frac{\mu_B}{\hbar} (g_{xx}^{(k)} + g_{yy}^{(k)} + g_{zz}^{(k)}), & A_{gk, \ell}^{0,0} &= -\sqrt{\frac{1}{3}} B_0 S_{kz}; \\ F_{gk, gk}^{2,0} &= -\sqrt{\frac{2}{3}} \frac{\mu_B}{\hbar} \left[g_{zz}^{(k)} - \frac{1}{2} (g_{xx}^{(k)} + g_{yy}^{(k)}) \right], & A_{gk, \ell}^{2,0} &= -\sqrt{\frac{2}{3}} B_0 S_{kz}; \\ F_{gk, gk}^{2, \pm 2} &= \frac{1}{2} \frac{\mu_B}{\hbar} (g_{xx}^{(k)} - g_{yy}^{(k)}), & A_{gk, \ell}^{2, \pm 2} &= 0. \end{aligned}$$

Similarly, the relevant components of the hyperfine tensor are:

$$\begin{aligned} F_{A_k, gk}^{0,0} &= -\sqrt{\frac{1}{3}} \frac{\mu_B}{\hbar} (A_{xx}^{(k)} + A_{yy}^{(k)} + A_{zz}^{(k)}), & A_{A_k, \ell}^{0,0} &= -\sqrt{\frac{1}{3}} S_{kz} I_{kz}; \\ F_{A_k, gk}^{2,0} &= -\sqrt{\frac{2}{3}} \frac{\mu_B}{\hbar} \left[A_{zz}^{(k)} - \frac{1}{2} (A_{xx}^{(k)} + A_{yy}^{(k)}) \right], & A_{A_k, \ell}^{2,0} &= -\sqrt{\frac{2}{3}} S_{kz} I_{kz}; \\ F_{A_k, gk}^{2, \pm 1} &= 0, & A_{A_k, \ell}^{2, \pm 1} &= \mp \frac{1}{2} S_{kz} I_{k\pm}; \end{aligned}$$

$$F_{A_k, gk}^{2, \pm 2} = \frac{1}{2} \frac{\mu_B}{\hbar} (A_{xx}^{(k)} - A_{yy}^{(k)}), A_{A_k, \ell}^{2, \pm 2} = 0.$$

In addition, when considered, the nuclear Zeeman term is given by $\sum_k F_{N_{k,l}}^{0,0} A_{N_{k,l}}^{0,0}$ with

$$F_{N_{k,l}}^{0,0} = \sqrt{3} \frac{g_n \mu_n}{\hbar}; \quad A_{N_{k,l}}^{0,0} = -\sqrt{\frac{1}{3}} B_0 I_{kz}.$$

The nuclear quadrupole term for ^{14}N nitroxide is neglected here. The second-rank tensors $F_{\mu, gk}^{2, M}$ are transformed in two steps: first, from the k th nitroxide g -tensor axes to the dipolar frame, with its z -axis coincident with the vector \mathbf{r} connecting magnetic dipoles, and then to the laboratory frame. The transformations from the dipolar frame to g -frame are defined by the Euler angles $\lambda_k \equiv (\alpha_k, \beta_k, \gamma_k)$ as shown in Figure 12.11 and the transformation from the laboratory frame to the dipolar frame, which is defined by $\eta \equiv (0, \theta, \phi)$. The transformed tensors are thus written as:

$$F_{\mu_k, l}^{L, M*} = \sum_{m', m''} D_{m', m''}^L(\eta) D_{m', m''}^L(\lambda_k) F_{\mu_k, gk}^{L, M}.$$

The Hamiltonian in the laboratory frame becomes:

$$H_0 = \sum_k [S_{kz} (C_k + A_k I_{kz} + B_k I_{k+} + B_k^* I_{k-}) + G_k I_{kz}],$$

where the coefficients C_k , A_k , G_k , and B_k are expressed as follows:

$$C_k = \sum_{m'} D_{0, m'}^2(\eta_k) K_{gk, m'}(\lambda_k), \quad A_k = \sum_{m'} D_{0, m'}^2(\eta_k) K_{A_k, m'}(\lambda_k);$$

$$2B_k = \sum_{m'} D_{1, m'}^2(\eta_k) K_{A_k, m'}(\lambda_k), \quad G_k = \gamma_{nk} B_0,$$

with

$$K_{\mu_k, m'}(\lambda_k) = [D_{m', 2}^2(\lambda_k) + D_{m', -2}^2(\lambda_k)] F_{\mu_k, g}^{2, 2} + D_{m', 0}^2(\lambda_k) F_{\mu_k, g}^{2, 0}$$

includes the transformations $D_{m', m''}^2(\lambda_k)$ from the dipolar frame to the k th magnetic frame. The explicit expressions for C_k , A_k , and B_k are unnecessary, since all the transformations were carried out numerically. They are listed by Saxena and Freed (1997). It is noted that the terms C_k , A_k , and B_k contain all anisotropies in the g and hf tensors as well as the Euler angles needed for their transformation from the respective principal-axes system to the laboratory frame. It is also noted that C_k , G_k , and A_k are real, whereas B_k is complex. Finally, it is noted that in carrying out the computations for B_0 well up to Q band (35 GHz), the nuclear Zeeman term can be safely omitted and the H_0 in real form can be obtained to a high accuracy based on the useful approximation described by Libertini and Griffith (1970).

Appendix 12.IV

Algorithm to Calculate Six-Pulse DQC Signal

The details of how to calculate the final density matrix, ρ_f , from which the DQC echo signal can be calculated as given by Equations 12.IV.3–12.IV.4 below, are given in this Appendix. Basically, this requires a series of transformations of the density matrix by a propagator, pulse or free evolution, and choosing the matrix elements of the density matrix after the application of a pulse on a coherence pathway. Here, the direct-product representation for $S_1 \otimes S_2 \otimes I_1 \otimes I_2$ will be used to express the matrix elements of the various operators as follows. To this end, the following details are required:

- i) **Matrix representation and notation:** For each electron, with spin $S = 1/2$, the matrix dimension is 2, whereas for each nucleus, with spin I , it is $(2I + 1)$, so that for the electron–nuclear spin coupled system of the nitroxide pair the size of the product space is $N \times N$ with $N = 4(2I_1 + 1)(2I_2 + 1)$, which becomes 36×36 for ^{14}N ($I = 1$) nitroxides. The Zeeman basis with the basis vectors $|k\rangle \equiv |m_1, m_2; M_1, M_2\rangle$ is employed here, where the $|k\rangle$ -values are the eigenvectors of the z -components of the electron and nuclear spin operators: $S_z|m\rangle = m|m\rangle$ and $I_z|M\rangle = M|M\rangle$. The basis states in the product space are described by lower-case Roman letters. Greek letters are used to describe the eigenvectors of H : $H|\alpha\rangle = \omega_\alpha|\alpha\rangle$. The diagonalization of the Hamiltonian, H , is accomplished by the unitary transformation $V^\dagger H V = E$, where E is a diagonal matrix of eigenvalues of H , and V^\dagger is the Hermitian adjoint of V . The eigenvectors of H are the columns of V : $|\alpha\rangle_k = \langle k|\alpha\rangle \equiv V_{k\alpha}$. In the computations the matrices E and V are the outputs of the matrix diagonalization subroutine, such as JACOBI (Press *et al.*, 1992), used here. (A better version of the JACOBI subroutine than that given by Press *et al.*, 1992 can be found on the Netlib website <http://netlib.org> or else is available from the authors.)
- ii) **Initial density matrix in product space:** Using the expression for $\rho(0)$ as given by Equation 12.13, the initial density matrix is expressed as

$$\rho(0) = (S_{1z} \otimes \mathbf{1}_2 + \mathbf{1}_1 \otimes S_{2z}) \otimes \mathbf{1}_{I_1} \otimes \mathbf{1}_{I_2}, \quad (12.IV.1)$$

where $\mathbf{1}_{I_1}$ and $\mathbf{1}_{I_2}$ are 3×3 unit matrices in the respective nuclear-spin spaces for ^{14}N nitroxides. A diagonal matrix of order 4×4 on the right-hand side of Equation 12.IV.1 represents $S_z \equiv S_{1z} + S_{2z}$ in the product space $S_1 \otimes S_2$ for the two nitroxide electron spins, that is $(\sigma_z \otimes \mathbf{1}_2 + \mathbf{1}_1 \otimes \sigma_z)/2 = \text{diag}(1, 0, 0, -1)$, where $\mathbf{1}_1$ and $\mathbf{1}_2$ are 2×2 unit matrices in the spin spaces for electrons 1 and 2, respectively.

- iii) **Transformation of the density matrix by a propagator.** The transformed density matrix, ρ' , under the action of a propagator is expressed as:

$$\rho' = e^{-iHt/\hbar} \rho e^{iHt/\hbar}. \quad (12.IV.2)$$

The following propagators are required: (i) pulse propagators, due to a $\pi/2$, or a π pulse; and (ii) free-evolution operators in the absence of a pulse. Figure 12.10

shows the effects of the various propagators, calculated using Equation 12.IV.3 below, employing the appropriate Hamiltonians and their durations. As an illustration, the procedure for a given density matrix, ρ , and the Hamiltonian, H , acting during the time period, t , is described here, which can be specialized for the various propagators by appropriate substitutions, with appropriate times t_k ($t_{1,2} = t_p$; $t_{3,4} = t_{DQ}$; $t_5 = t_m - t_p$; $t_6 = t_5 + t_{\text{echo}}$) and Equations 12.17–12.21, which describe the Hamiltonians used in the analysis of the six-pulse DQC sequence.

The matrix elements of ρ' in Equation 12.IV.2 can be expressed as $\rho'_{jk} = e^{-iH_{jm}t} \rho_{mn} e^{iH_{nk}t} = V_{j\alpha} e^{-i\omega_\alpha t} V_{m\alpha}^* \rho_{mn} V_{n\beta} e^{-i\omega_\beta t} V_{k\beta}^*$, since $e^{-iH_{km}t} = V_{k\alpha} e^{-i\omega_\alpha t} V_{\alpha m}^*$. The required summations are carried out over the repeating indexes, or explicitly

$$\rho'_{jk} = \sum_{\alpha, \beta, m, n} \rho_{mn} V_{m\alpha}^* V_{n\beta} V_{j\alpha} V_{k\beta}^* e^{-i\omega_{\alpha\beta} t} \quad (12.IV.3)$$

with $\omega_{\alpha\beta} \equiv \omega_\alpha - \omega_\beta$. Equation 12.IV.3 can be written using a short-hand notation as $\rho' = L\rho$. In this notation, L is an operator, which is Q for a free evolution period or R for the action of a pulse. Coherence pathway selection implies retaining only those elements of ρ' , which belong to the pathways of interest, with the subsequent summation conducted over all pathways that contribute to the echo of interest. In computations this is accomplished by retaining only those matrix elements that correspond to the selected pathway, setting the rest to zero. This may be expressed as the application of a projection operator P (which, in reality, does not need to be constructed). The final density matrix after application of N pulses and subsequent evolution periods is then calculated as

$$\rho_f(t) = \sum_{\{p_k\}} (Q_N P_{p_N} R_N, \dots, Q_1 P_{p_1} R_1) \rho(0) \quad (12.IV.4)$$

The product is computed for the full set of coherence pathways $\{p_k\}$ that contribute to the echo and the sum is then taken to be finally used in computing of $\text{Tr}[\rho_f S_+]$

- iv) **Coherence pathway selection:** Subsequent to the action of a pulse propagator, of the matrix elements as calculated in (iii) above, all but those in the electronic product subspace of the density matrix ρ that correspond to selected coherence order p should be set to zero. The correspondence of ρ_{ik} to p is compiled in Table 12.IV.1 pertinent to the coherence pathways depicted in Figure 12.10 illustrating the coherence pathways of the six-pulse DQC sequence. This selection of coherence pathways is achieved experimentally through phase cycling (Borbat and Freed, 2000), or in computations is based on Table 12.IV.1.

Appendix 12.V Approximate Analytic Expressions for 1-D DQC Signal

For completeness, the equation given by Borbat and Freed (2000), used for making the comparison with 1-D DQC signals produced in rigorous computations, is

included here. The echo amplitude, V , is a function of $t_{dip} = 2t_p - t_m$, and is given by

$$V(t_{dip}) = K(\omega_1)K(\omega_2)F(t_p)F(t_m - t_p). \quad (12.V.1)$$

The time variables are defined in accordance with Figure 12.10, and the notations are defined in the text. $F(t)$ is expressed as:

$$F(t) = (p^2 + q^2 \cos Rt) \cos At - q \sin Rt \sin At. \quad (12.V.2)$$

In Equation 12.V.2, $q = b/R$ and $p^2 = 1 - q^2$; $A = d(1 - 3 \cos^2 \theta)$ and $b = -A/2$, where A and b represent the secular and pseudosecular parts of the dipolar coupling; $R^2 = \Delta\omega^2 + b^2$, where $\Delta\omega = \omega_1 - \omega_2$ is the difference between the Larmor frequencies ω_1 and ω_2 of the nitroxide's electron spins in the frame of reference rotating with the frequency ω_f of the excitation pulses, set to coincide are expressed in the simplest form as

$$K(\omega_k) = \left(\frac{\omega_{1f}^2}{\Delta\omega_k^2 + \omega_{1f}^2} \sin^2 \left(\frac{\pi}{2} \sqrt{1 + \Delta\omega_k^2 / \omega_{1f}^2} \right) \right)^3, \quad (12.V.3)$$

where $\omega_{1f} = \gamma_e B_1$ for π pulses, which are all taken to be equal to each other, although in general they need not be.

The powder averaging is carried out essentially in the same way as in the rigorous computations, with ω_k determined for each set of (M_1, M_2) , since $\omega_k = \omega_k(\lambda_k, \eta)$. This was determined using an approximation given by Libertini and Griffith (1970).